UNIVERSITÀ DEGLI STUDI DI CATANIA

Dipartimento di Ingegneria Elettrica Elettronica e Informatica

XXVI Ph.D. Course in Systems Engineering

Pappalardo Fulvio Livio

Fractional Order Systems: $PI^{\lambda}D^{\mu}$ Controller Design and Fractional Order Elements Modeling

---

Ph.D. Thesis

Coordinator: *Prof. L. Fortuna*

Tutor: *Prof. R. Caponetto*

To Me and to Anyone who believed in me

Synopsis

Can the meaning of derivatives with integer order be generalized to derivatives with non-integer orders?

> With these few words, in 1695, Leibniz rised to L'Hôpital, for the very first time, the question of Non-Integer Order derivative. The answer was:

What if the order will be 1/2?

In this way was born an ongoing topic studied for more than 300 years and that today is noticed as Fractional Caclulus, that is the calculus of integrals and derivatives of any arbitrary real or complex order. It's importance is demonstrated in widespread flieds of science and engineering. In fact fractional integrals and derivatives are applied in the theory of control and modeling of dynamical systems, when the controlled system and/or the controller is described by a fractional differential equations. Important field of interest for fractional calculus are Fluid Flow, Electrical Networks, Chemical Physics, Optics and Signal Processing. This research thesis within the XXVI Ph.D. Course in

Systems Engineering is centered on Fractional, or also noticed as Non-Integer Order, Systems. The Ph.D. Thesis' purpose is to present the auto-tuning procedure of Fractional Order PID Controllers ($PI^{\lambda}D^{\mu}$) proposing also a future implementation via fractional order elements. The Thesis is organized in four chapters to outline the different research activity phases developed during the Ph.D. course. In the Chapter 1 an overview on Fractional Order Systems is presented. The Chapter 2 focuses on the auto-tuning procedure proposed for Non-Integer Order Proportional-Integral-Derivative (PID) controllers and some examples are presented. The Chapter 3 is divided in two parts: the first one is dedicated to the modeling and control of Ionic Polymer Metal Composite (IPMC) and than a study on Fractional Order Elements modeling as possible building block for controller implementation is proposed. Finally the conclusions are presented in the Chapter 4.

Contents

1

Fractional Calculus and Fractional Order Systems

In this chapter a brief introduction on Fractional Calculus and Fractional Order Systems is given. This chapter's aims is to present and remind some fundamental theoretical notions on applications and implementations of fractional order systems throw some historical notes and definitions.

1.1 Fractional Order Differintegral Operator: Historical Notes

Until 1695 the derivative calculus was identified with the operator $D = \frac{d}{dx}$ and the nth derivative of a function f was expressed by $D^n f(x) = \frac{d^n f(x)}{dx^n}$ where n must be defined as a positive integer number. Thanks to a cross talk between L'Hôpital and Leibniz, in which the first one asked, in 1695, what meaning could be assumed from $D^n f$ if n was non integer, the study of fractional calculus began to affect many mathematicians like Euler, Laplace, Fourier, Abel, Liouville and Riemann. The process of born of modern fractional calculus takes from 1695 until 1884 when was included in this theory the operator D^m, where m could be rational or irrational, positive or negative, real or complex [1]. My researches on fractional order systems and their applications allow me to understand how important is the fractional calculus and its application in a very large scale even outside mathematics fields like design of heat-flux meters, bioengineering and artificial muscles design, dissemination of atmospheric pollutants and so on. One of the most relevant characteristics of fractional derivatives is to well describe memory and hereditary of materials properties in comparison with integer order modeling. It also allow to justify many behaviors that a classic mathematical approach doesn't explain. The fractional approach in derivatives and integrals was unexplored in engineering, because of its complexity, the apparent self-sufficiency of the integer order calculus and the fact that it does not have a fully acceptable

geometrical or physical interpretation. Moreover it represents more accurately some natural behavior related to different areas of engineering, bioengineering [2, 3], viscoelasticity [4, 5, 6], robotics [7, 8, 9], control theory [10, 11] and signal processing [12, 13, 14]. Fractional integrals and derivatives also appear in the theory of control of dynamical systems [15, 16] that present some intrinsic fractional order behavior that needs fractional order calculus to be explained. To represent systems with nonlinear complex phenomena and high-order dynamics the Fractional Order approach could be useful because the arbitrary order of derivatives gives more tools to explain a specific behavior. It is also important the fact that fractional order derivatives depend on all the history of the system. The nonlocal characteristics like *infinite memory* in the behavior of real dynamical systems, in fact allows the fractional calculus to take relevance in engineers' attention [17, 18, 19]. To implement fractional derivative functions in logical circuit there are three different strategies to simulate fractional order systems [26, 27]:

- *Computational methods based on the analytic equation* that present multiple parameters and could be very difficult to analyze because any single point in function history must be analyzed.
- *Approximation through a rational system in discrete time* that replace the analytical system with the equivalent in frequency space discrete one. Those methods suggest to truncate the model in time domain and require the same number of coefficients as samples to the detriment of the characteristic of *infinite memory*.

- *Approximation of the fractional system using rational function in continuous time* that approximate by rational continuous approach truncating the series and for this reason it must be limited to a specific frequency range of operation as it is shown in next chapters.

From the electronic point of view other three methods using analogical circuit with fractional order behavior could be introduced to obtain the response of a fractional order system:

- *Component by component implementation* [24] in which the approximation of the Transfer Function is done by a recursive Low Pass Filter circuit. Unfortunately this approach presents a limited frequency band of work and a poor accuracy given by the approximation itself.
- *Field Programmable Analog Array (FPAA)* [62] that allows to change the fractional order system dynamical behavior modifying the FPAA circuit.
- *Fractional order impedance component* using a capacitor with fractional order behavior [29].

1.2 Review on Preliminaries and Definitions

From a mathematica point of view, fractional, or non integer order, systems can be considered as a generalization of integer order systems [20], [21]. As previously introduced, the derivative and integral operator could be generalized with the following notation:

$$D^{\alpha} = \begin{cases} \frac{\partial^{\alpha}}{\partial t^{\alpha}} & \alpha > 0 \\ 1 & \alpha = 0 \\ \int_a^t (d\tau)^{-\alpha} & \alpha < 0 \end{cases} \tag{1.1}$$

with $\alpha \in \Re$. The study of fractional systems may be approached in the time domain by using the following non integer order integration operator [22]:

$$\frac{\partial^{-m} h(t)}{\partial t^{-m}} = \frac{1}{\Gamma(m)} \int_0^t (t-y)^{m-1} h(y) dy \tag{1.2}$$

Many mathematicians have formulated equations to describe fractional order behavior, but the most frequently used for the general fractional differintegral are the following tree [20, 22]:

- *Grunwald-Letnikov*:

  Derivative:

$$D^{\alpha} f(t) = \lim_{h \to 0} \frac{1}{h^{\alpha}} \sum_{m=0}^{[\frac{(t-\alpha)}{h}]} (-1)^m \frac{\Gamma(\alpha+1)}{m!\Gamma(\alpha-m+1)} f(t-mh) \tag{1.3}$$

  Integral:

$$D^{-\alpha} f(t) = \lim_{h \to 0} h^{\alpha} \sum_{m=0}^{[\frac{(t-\alpha)}{h}]} \frac{\Gamma(\alpha+m)}{m!\Gamma(\alpha)} f(t-mh) \tag{1.4}$$

  where [.] means the integer part and $h(t)$ may be any function for which the integral in (1.2) exists.

- *Riemann-Liouville*:

  Derivative:

$$D^{\alpha}f(t) = \frac{1}{\Gamma(n-r)}\frac{d^n}{dt^n}\int_a^t \frac{f(\tau)}{(t-\tau)^{r-n+1}}d\tau \tag{1.5}$$

Integral:

$$I_c^{\alpha}f(t) = \frac{1}{\Gamma(\alpha)}\int_c^t \frac{f(\tau)}{(t-\tau)^{1-\alpha}}d\tau \tag{1.6}$$

with $(n-1 < r < n)$ and where $\Gamma(.)$ is the *Gamma* function.

- *Caputo*:

$$D^{\alpha}f(t) = \frac{1}{\Gamma(m-\alpha)}\int_0^t \frac{f^{(m)}(\tau)}{(t-\tau)^{\alpha-m+1}}d\tau \tag{1.7}$$

with $(n-1 < r < n)$.

In the Riemann-Liouville and Caputo definition it appears the factorial function $\Gamma(.)$ defined by:

$$\Gamma(m) = \int_0^{\infty} e^{-u}u^{m-1}du \tag{1.8}$$

defined for positive real m. The definition of fractional derivative easily derives from(1.2) by taking a suitable integer n order derivative and a suitable non integer m order integral to obtain an $n-m=q$ order one:

$$\frac{\partial^q f(t)}{\partial t^q} = \frac{\partial^{n-m} f(t)}{\partial t^{n-m}} = \frac{1}{\Gamma(m)}\frac{\partial^n}{\partial t^n}\int_0^t (t-y)^{m-1}f(y)dy \tag{1.9}$$

that becomes the canonical first order derivative if $q=1(n=2, m=1)$.

1.3 Fractional Calculus in Laplace Domain

As it is known, it is often convenient to perform the analysis of systems dynamical behaviors in the frequency domain. For that reason it is necessary to highlight that the Laplace Transform of fractional derivatives has not so big differences respect to the integer one. Same considerations could be done on the Inverse Laplace Transformation in case of systems with only frequency response known. Generally, the Laplace Transform is defined with the following equation [23, 24]:

$$\mathcal{L}\{D_t^\alpha f(t)\} = s^\alpha \mathcal{L}\{f(t)\} - \sum_{k=0}^{n-1} s^k [D^{\alpha-j-1} f(0)] \tag{1.10}$$

where n is an integer such that $n-1 < \alpha < n$. It can be noticed that this transform takes into account all initial conditions from the first to the $n^{th}-1$ derivative. In that case we can obtain the same expression for the Fourier Transform if s is replaced with jw. It also could be noticed that if all the derivatives are zero the expression would be simplified with the following one:

$$\mathcal{L}\{D_t^\alpha f(t)\} = s^\alpha \mathcal{L}\{f(t)\} = s^\alpha F(s) \tag{1.11}$$

Likewise the non integer order integrators $1/s^\alpha$ could be easily obtained replacing α with $-\alpha$ and considering $f(t) = \delta(t)$, the Dirac impulse. In this case, using the Caputo definition 1.7, we obtain:

$$\mathcal{L}\left\{\frac{t^{\alpha-1}}{\Gamma(\alpha)}\right\} = \frac{1}{s^\alpha} \tag{1.12}$$

and its Inverse Laplace Transform:

$$\mathcal{L}^{-1}\left\{\frac{1}{s^{\alpha}}\right\} = \frac{t^{\alpha-1}}{\Gamma(\alpha)} \tag{1.13}$$

From this equation it could be easily obtained the generic fractional system impulse response equation:

$$\mathcal{L}^{-1}\left\{\frac{k}{(s+a)^{\alpha}}\right\} = k\frac{t^{\alpha-1}e^{-at}}{\Gamma(\alpha)} \tag{1.14}$$

In systems theory is important to obtain a time domain representation of the impulse response of a system (Y(s)/U(s)). It is notice that from the 1.11 combined with the 1.14 we can obtain:

$$\frac{Y(s)}{U(s)} = \frac{1}{(s+a)^{\alpha}} \Rightarrow (s+a)^{\alpha}Y(s) = U(s) \tag{1.15}$$

that becomes:

$$s^{\alpha}Y(s-a) = U(s-a) \tag{1.16}$$

if substituting s with $(s-a)$.

Applying the Inverse Laplace Transform we obtain:

$$\mathcal{L}^{-1}\{s^{\alpha}Y(s-a)\} = \mathcal{L}^{-1}\{U(s-a)\} \Rightarrow \frac{\partial^{\alpha}}{\partial t^{\alpha}}[e^{at}y(t)] = e^{at}u(t) \tag{1.17}$$

So we have obtained a non integer order differential equation with a finite number of terms that has, both for system input and output,

an exponential time dependence. If we want to explain that system in the common time-varying state space representation:

$$\begin{cases} \frac{\partial^\alpha x(t)}{\partial t^\alpha} = A(t)x(t) + B(t)u(t) \\ y(t) = C(t)c(t) + D(t)u(t) \end{cases} \tag{1.18}$$

we must have $A(t) = 0, B(t) = e^{at}, C(t) = e^{-at}$ and $D(t) = 0$.

1.4 Geometrical Interpretation

As it is noticed, a geometrical explanation in integral order calculus that relates some physical quantities, for example, the relationship between position and speed of an object to explain the instant rate of change of a function, is well-accepted. Unfortunately in fractional order calculus, some geometrical interpretation has been proposed only since last decade. One of them proposes a probabilistic explanation using the Grünwald-Letnikov definition in 1.3 and 1.4 [25]. If:

$$0 < \alpha < 1 \tag{1.19a}$$

$$\gamma(\alpha, m) = (-1)^m \frac{\Gamma(\alpha + 1)}{m!\Gamma(\alpha - m + 1)} \tag{1.19b}$$

the value of the function at present time is obtained if $m = 0$, while if $m > 0$:

$$-\sum_{m=1} \gamma(\alpha, m) = 1 \tag{1.20}$$

We can noticed that if $m \neq 0$ the value of γ vanishes it the analysis point is far from present. Therefore, the expected value of a random variable X could be expressed by:

$$-\sum_{m=1}^{\inf} \gamma(\alpha, m) x(t - mh) \tag{1.21}$$

where:

$$P(X = x(mh)) = |\gamma(\alpha, m)| \tag{1.22}$$

with $m = 1, 2, ...$ and $0 < \alpha < 1$. In this case values near the present time have a bigger weight on the results than the far ones as it is shown in Fig. 1.1

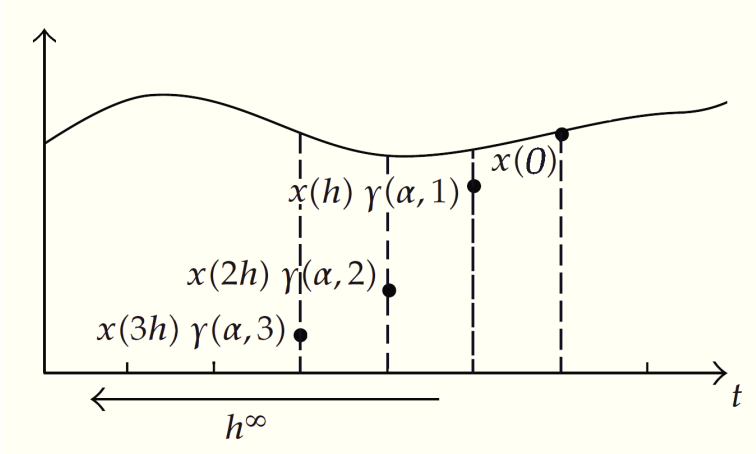

Fig. 1.1. Tenreiro fractional order derivative interpretation.

1.5 Most Important Properties of Fractional System

One of the most important tool in system and control theory is the Bode analysis trough Bode Diagrams that allow to study fractional order systems using the same criteria adopted for integer order ones. As well as integer systems, the common Laplace-like Transfer Function of a fractional system could be written as follow:

$$G(s) = \frac{Y(s)}{U(s)} = \frac{b_m s^{\beta_m} + b_{m-1} s^{\beta_{m-1}} + ... + b_0 s^{\beta_0}}{a_n s^{\alpha_n} + a_{n-1} s^{\alpha_{n-1}} + ... + a_0 s^{\alpha_0}} \tag{1.23}$$

where $\alpha, \beta \in \Re$, $\beta_0 < ... < \beta_{m-1} < \beta_m$ and $\alpha_0 < ... < \alpha_{n-1} < \alpha_n$. Analyzing the Transfer Function:

$$F(s) = \frac{k}{(s+a)^\alpha} \tag{1.24}$$

and assuming $s = j\omega$, we obtain:

$$F(j\omega) = \frac{k}{(j\omega+a)^\alpha} = \left[\frac{k^{1/\alpha}}{(j\omega+a)}\right]^\alpha = \left[\frac{k^{1/\alpha}}{a}\frac{1}{(1+\frac{j\omega}{a})}\right]^\alpha \tag{1.25}$$

that in a Magnitude/Phase notation could be written as:

$$F(j\omega) = \left|\frac{k^{1/\alpha}}{a}\frac{1}{(1+\frac{j\omega}{a})}\right|^\alpha e^{j\alpha\angle\left[\frac{k^{1/\alpha}}{a}\frac{1}{(1+\frac{j\omega}{a})}\right]} \tag{1.26}$$

from which Bode Magnitude and Phase could be calculated with:

$$\left|F(j\omega)\right|_{dB} = 20log_{10}\left[\frac{k^{1/\alpha}}{a}\frac{1}{\sqrt{1+\omega^2/a^2}}\right]^\alpha \tag{1.27}$$

$$\angle F(j\omega) = \alpha \angle \left[\frac{k^{1/\alpha}}{j\omega/p + 1} \right] = -\alpha \arctan \frac{\omega}{p} \tag{1.28}$$

These equation leads to the diagrams reported in Figg. 1.2 and 1.3

It is quite evident that the fractional order α modulates the slope of the magnitude diagram providing a useful parameter for open loop synthesis of the controller and in the meanwhile modulates the scale of the phase law leading the phase angle approach to $-\alpha\pi/2$ for $\omega \to \infty$. To consider the impulse canonical responses of a fractional order system, the (1.14) could be taken into account and written as follow:

$$f(t) = L^{-1}\left\{ \frac{k}{(s/p+1)^{\alpha}} \right\} = L^{-1}\left\{ \frac{kp^{\alpha}}{(s+p)^{\alpha}} \right\} = kp^{\alpha}\frac{t^{\alpha-1}e^{-pt}}{\Gamma(\alpha)} \tag{1.29}$$

It could be easily noticed that if $\alpha < 1$ and $t \to 0$, $f(t)$ is infinite as it is shown in Fig. 1.2, but the step response can be calculated for any positive α accordingly to the Cauchys theorem hypothesis on the existence of the integral [30]. In fact if the Incomplete Gamma Function definition is introduced as follows:

$$\Gamma(\alpha, x) = \int_0^x e^{-y} y^{\alpha-1} dy \tag{1.30}$$

the step response of fractional system can be calculated by:

$$g(t) = \int_0^t f(t)dt = k\frac{\Gamma(\alpha, pt)}{\Gamma(\alpha)} \tag{1.31}$$

As it is shown in Fig. 1.4, all those applications, like fast control schemes [31] or image processing [32], in which a high speed is required

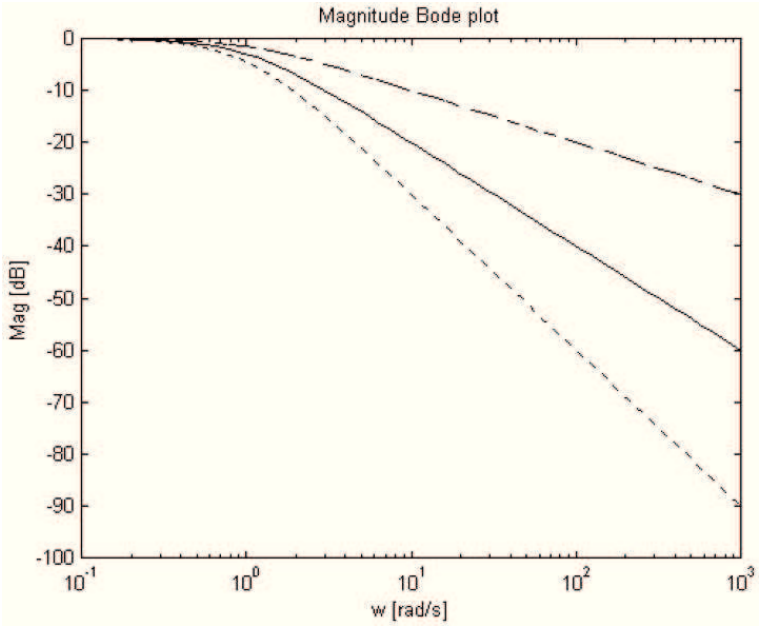

Fig. 1.2. Magnitude Bode Plot of fractional system $F(s) = 1/(s+1)^{\alpha}$ with $\alpha = 1$ (solid), $\alpha = 0.5$ (dashed), $\alpha = 1.5$ (dotted).

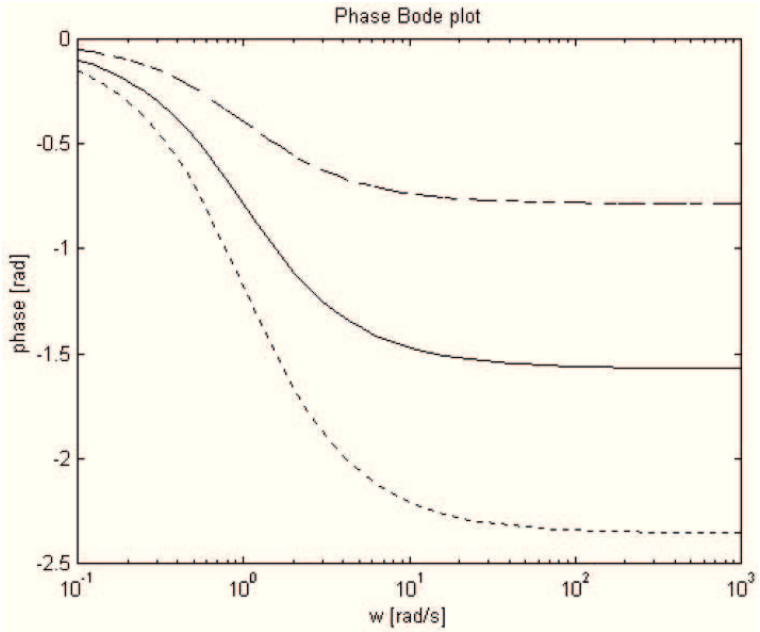

Fig. 1.3. Phase Bode Plot of fractional system $F(s) = 1/(s+1)^{\alpha}$ with $\alpha = 1$ (solid), $\alpha = 0.5$ (dashed), $\alpha = 1.5$ (dotted).

could be successfully exploited accordingly to the faster response of systems with $\alpha < 1$ and the infinite value of the derivative for $t = 0$.

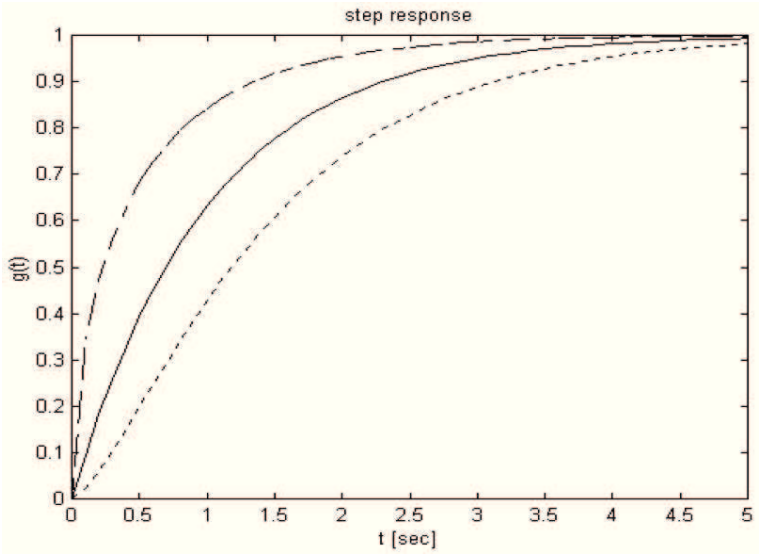

Fig. 1.4. Step response of a fractional system for different values of α (dashed) $\alpha = 0.5$, (solid) $\alpha = 1$, (dotted) $\alpha = 1.5$.

1.6 Impulse Response of a Generic Non-Integer Order System

In time domain analysis there are several examples of systems that can be explained by the following transfer function:

$$F(s) = \frac{X(s)}{U(s)} = \frac{k}{s^{\alpha} + a} \tag{1.32}$$

The inverse Laplace transform of this equation is not analytically derivable, but a series expansion of it can be easily obtained. As it is known the previous equation could be written as:

$$F(s) = \frac{k}{s^\alpha + a} = \frac{k}{s^\alpha} \sum_{n=0}^{\infty} \frac{(-a)^n}{s^{n\alpha}} \tag{1.33}$$

Applying the (1.13) to each term of the sum the following equation is obtained:

$$f(t) = \mathcal{L}^{-1}\left[\frac{k}{s^\alpha} \sum_{n=0}^{\infty} \frac{(-a)^n}{s^{n\alpha}}\right] = kt^{\alpha-1} \sum_{n=0}^{\infty} \frac{(-a)^n t^{n\alpha}}{\Gamma(n\alpha + \alpha)} \tag{1.34}$$

that represents he impulse response and whose graphs for different values of α with $a = k = 1$ are shown in Fig. 1.5

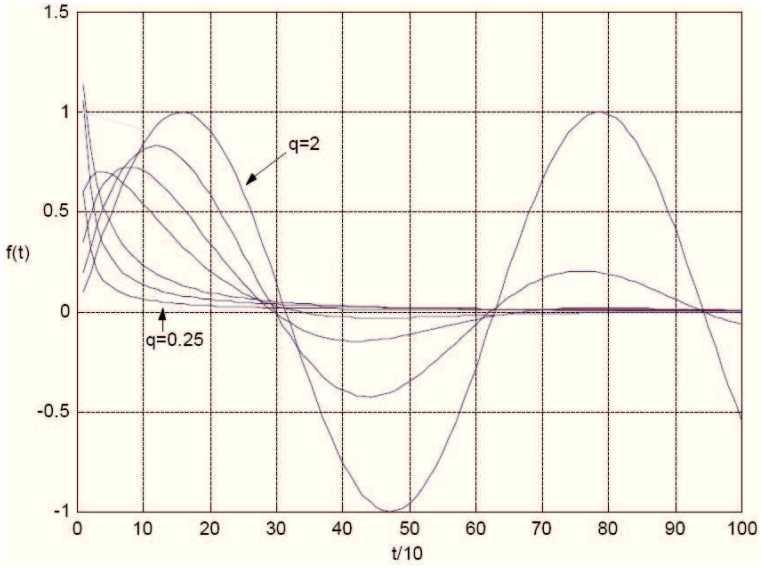

Fig. 1.5. Impulse response of $f(t)$ with α varying from 0.25 to 2 in 0.25 increments.

2

Auto-tuning procedure of Fractional Order PID Controllers

This chapter focuses on the introduction of an auto-tuning procedure for fractional order $PI^{\lambda}D^{\mu}$ controllers. The tuning procedure is developed into tree main steps: at first a Relay-Test was performed to identify the process, in the next step the $PI^{\lambda}D^{\mu}$ parameters are calculated to satisfy project specs of phase margin (ϕ_m)and cut-off frequency (ω_{cg}), in the end closed loop step response performances of the $PI^{\lambda}D^{\mu}$ controller is evaluated. To highlight the ductility of $PI^{\lambda}D^{\mu}$ controllers instead of integer PID some simulations were performed and presented at the end of this chapter. In the first section a brief introduction on the characterization procedure of a $PI^{\lambda}D^{\mu}$ controller designed to stabilize a first-order plant with delay-time is presented. In the second section the *Relay-Test* auto-tuning method is introduced and through a feedback algorithm it is also described the routine adopted to design the $PI^{\lambda}D^{\mu}$ accordingly to the project specifications of phase margin and cross-over frequency [33]. In the third sec-

tion the performances are evaluated through two examples of closed loop step response [34].

2.1 Design procedure of a Fractional Order PID Controller

The increasing interest on $PI^{\lambda}D^{\mu}$ tuning techniques could be justified to the widespread industrial use of PID controllers and their non-integer order representation potentiality. A new procedure to define the parameters of fractional order $PI^{\lambda}D^{\mu}$ controllers that stabilize a plant with delay-time is introduced in this section. The study of fractional order dynamical systems in control systems theory and practice has been marginally due to the absence of mathematical methods. In last ten years a grown of interest has been registered and the first systematic approaching is the three CRONE (*Commande Robuste d'Ordre Non Entier*) control generations that represent the framework for fractional order system application in that area [31], [35], [36], [37]. The first paper on $PI^{\lambda}D^{\mu}$ could be associated to Igor Podlubny [12] in which he demonstrated a better response in controlling fractional order systems than classical PID. After this, other authors have studied this matter and focused on some important aspects of this fractional systems [38], [39], [40]. In these last papers an analog implementation of non integer order integrator based on Field Programmable Analog Array (FPAAs) has proposed to implement a $PI^{\lambda}D^{\mu}$ controller. During the last decades, numerous methods, even based on characterizing the dynamic response of plants using first-order model with time delay, has been developed for setting P, PI and PID controllers parameters. The approach developed in [41], in which a generalization of the Hermite-

Biehler theorem was derived to compute the set of all stabilizing PID controllers for a given linear and time invariant plant, constitutes the first attempt to find a characterization of these systems.

The aim of this thesis is to find a complete solution to the characterizing set problem of non integer order $PI^{\lambda}D^{\mu}$ controllers applied to Fractional Order Systems (FOS), fixing previously the fractional orders of the integrative (λ) and derivative (μ) actions.

In the following a new auto-tuning procedure of Fractional Order PID Controllers is proposed. A first order process with a time delay could be modeled with the following Transfer Function:

$$G(s) = \frac{k}{1+Ts}e^{-Ls} \tag{2.1}$$

were k is a steady-state gain of the plant, L is the time delay and T is the time constant of the plant. The generic step response of that system is shown in Fig. 2.1.

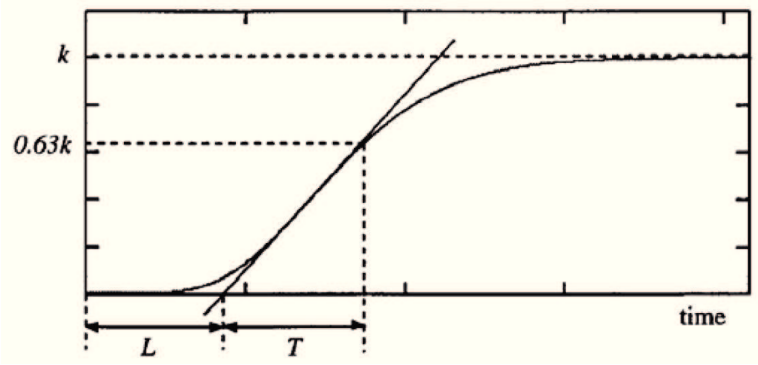

Fig. 2.1. Open-loop step response.

A fractional order PID controller could be modeled by the formula (2.2), as introduced in [12].

$$C(s) = PI^{\lambda}D^{\mu} = K_p + K_i\frac{1}{s^{\lambda}} + K_d s^{\mu} \tag{2.2}$$

were λ is the the integrator order and μ is the differentiator order ($\lambda, \mu \in \mathbb{C}$). If it is assumed u as command signal, y as plant output and $G(s)$ the plant to be controlled by the controller $C(s)$, the feedback control system could be represented by the diagram in Fig. 2.2.

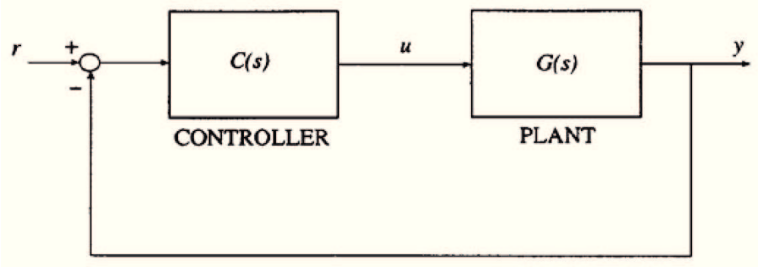

Fig. 2.2. Feedback control system.

As explained in [45] and [46], the extension of derivation and integration orders from integer to complex numbers provides a more flexible tuning strategy and therefore an easier way to achieve control requirements with respect to classical PID controllers. Another approach, described in [47] and [48], is characterized by the use of a new strategy to control first-order systems having a long time delay. In this last work it has been applied a robustness constraint which allow to force the phase of the open-loop system to be flat at the gain crossover frequency. The main drawback of $PI^{\lambda}D^{\mu}$ auto-tuning algorithm lies in the following

[49]: during the phase of plant identification at a frequency with a phase lower than $-180°$ (plant of order greater than two), it is required to look for a negative value for the delay in the auto-tuning equation. In this section it has described the improved relay test routine that allows to overcome this limitation. From a designer point of view, given the desired crossover frequency ω_{cg} and phase margin φ_m, the proposed procedure allows to design a $PI^{\lambda}D^{\mu}$ controller able to ensure a closed loop system which is both robust versus gain variations and with an iso-damping step response. Commercial auto-tuned controllers are based on PID structure and could be divided in two main families accordingly to their tuning technique:

- 1^{st} or 2^{nd} Ziegler-Nichols method based on the opened/closed loop step response with not tuned controller
- *Relay-Test* method based on a feedback loop with periodic output oscillation controlled by a relay

These two main categories differ also in controller synthesis methods, algorithm used to set parameters or the plant dynamic.

2.1.1 Plant Identification and Controller Auto-Tuning

Considering D^{μ} as the non integer order derivative and $D^{-\lambda}$ as the non integer order integration in time domain [50], [51] and K_p, K_i and K_d as control action coefficients, the $PI^{\lambda}D^{\mu}$, whose block diagram is shown in Fig. 2.3, could be model with (2.3):

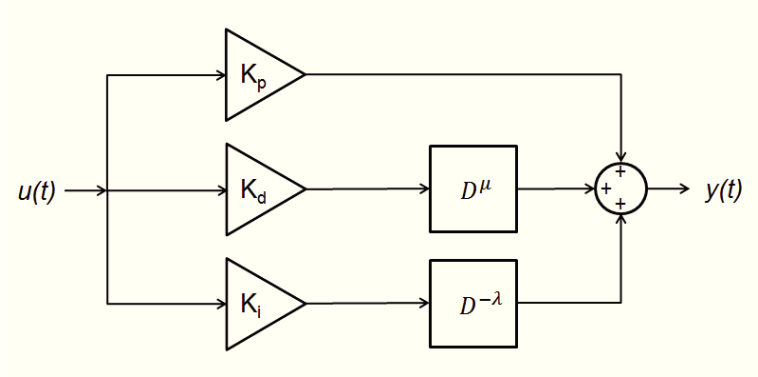

Fig. 2.3. Fractional Order PID block diagram.

$$y(t) = K_p + K_i D^{-\lambda} u(t) + K_d D^{\mu} u(t) = K_p \left[1 + \frac{K_i}{K_p} D^{-\lambda} + \frac{K_d}{K_p} D^{\mu} \right] u(t) \tag{2.3}$$

It is clear that the Laplace Transfer Function of the (2.3) rise to (2.4):

$$PI^{\lambda}D^{\mu}(s) = \frac{Y(s)}{U(s)} = K_p \left[1 + \frac{1}{T_i} s^{-\lambda} + T_d s^{\mu} \right] \tag{2.4}$$

were $T_i = K_p/K_i$ and $T_d = K_d/K_p$ are integrative and differential time constants. As integer order PID, the three actions (proportional, integrative and derivative) play a main rule in the design of the $PI^{\lambda}D^{\mu}$ controller because, as it is known, the proportional one (K_p) sets the crossover frequency ω_{cg} without modifying the phase margin, the integral one (K_i) reduces noises and steady state errors, but leads to a rise of the overshoot and a reduction of phase margin that are stabilized by the derivative action (K_d). To satisfy specifications on phase margin φ_m and crossover frequency ω_{cg}, the control system designed in Fig. 2.4 was studied and implemented.

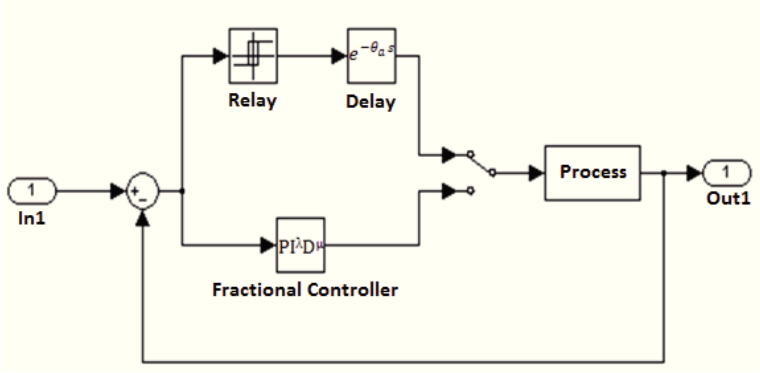

Fig. 2.4. Block diagram of the closed loop system.

The auto-tuning procedure has been divided into two steps. The fist one, the *Relay-test phase*, was used to identify the process at the desired crossover frequency, while the second one, the $PI^{\lambda}D^{\mu}$ *Auto-tuning phase*, allowed to determine the controller parameters in order to ensure a robust and iso-damping system response. After these phases of identification and auto-tuning (Relay and Delay blocks in Fig. 2.4) the switch is commuted on the designed $PI^{\lambda}D^{\mu}$ controller and the system works in closed loop form.

2.1.2 Relay-test phase

The choice of relay feedback is motivated by the possible integration of the system identification and control both in the algorithm and into the control device. It is noticed that if a system rise the stability limit the pure imaginary poles give to the system a periodicity and the system start to oscillate with a magnitude depending on starting conditions. If another parametric variation take place, the imaginary poles assume

a little real value and than the oscillation runs to infinite. As it is shown in Fig. 2.4, in the direct chain an ideal relay with a symmetric instantaneous nonlinearity was inserted. If a sinusoidal signal $\sin(t) = A\sin(\omega_t)$ is applied, the output is a periodic signal $w(t)$ with the same frequency of the input one and a $\pm d$ amplitude. This output signal could be therefore written in Fourier series as follow:

$$w(t) = \sum_{n=1}^{\infty}(A_n \sin(n\omega_t) + B_n \cos(n\omega_t)) \tag{2.5}$$

Due to the low pass filter behavior of the system, the higher order harmonics could be skipped and than the (2.5) could be approximate to:

$$\tilde{w}(t) = A_1 \sin(\omega_t) + B_1 \cos(\omega_t)) \tag{2.6}$$

were:

$$A_1 = \frac{1}{\pi}\int_0^{2\pi} \tilde{w}(t)\sin(\omega_t)\, d\omega_t \tag{2.7}$$

$$B_1 = \frac{1}{\pi}\int_0^{2\pi} \tilde{w}(t)\cos(\omega_t)\, d\omega_t \tag{2.8}$$

Assuming than:

$$Y = \sqrt{A_1^2 + B_1^2} \tag{2.9a}$$

$$\varphi = arctg(\frac{B_1}{A_1}) \tag{2.9b}$$

the (2.6) could be written as:

$$\tilde{w}(t) = Y \sin(\omega_t + \varphi) \tag{2.10}$$

Than the descriptive function $N(A)$ associated to the nonlinearity could be formulated by:

$$N(A) = \frac{Y e^{j\varphi}}{A} \tag{2.11}$$

As it is shown in Fig. 2.5 the output signal is a square wave with $\pm d$ amplitude.

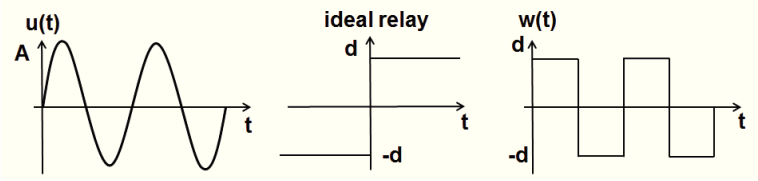

Fig. 2.5. Ideal Relay I/O behavior.

From the (2.7) and (2.8) it is obtained:

$$A_1 = \frac{1}{\pi}\int_0^{2\pi} \tilde{w}(t)\sin(\omega_t)\, d\omega_t = \frac{1}{\pi}\int_0^{2\pi} d(t)\sin(\omega_t)\, d\omega_t = \frac{4d}{\pi} \tag{2.12a}$$

$$B_1 = 0 \tag{2.12b}$$

and than the (2.11) could be evaluated as:

$$N(A) = \frac{4d}{\pi A} \tag{2.13}$$

Once the descriptive function was evaluated, it was used to replace the ideal relay in the system control chain as it is shown in Fig. 2.6

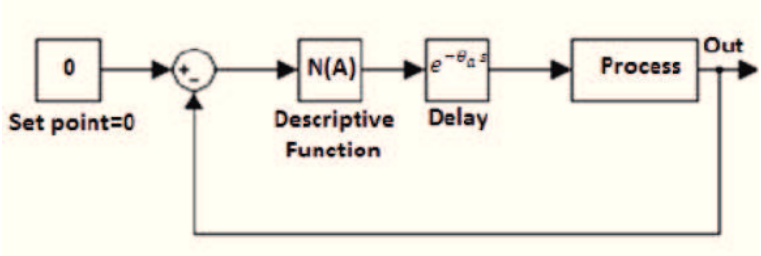

Fig. 2.6. Relay-test block diagram.

Considering a null reference signal and skipping the direct chain delay, it is obtained:

$$y = N(A)G(j\omega)e = N(A)G(j\omega)(-y) \tag{2.14}$$

were e is the error between the reference and the output signals and $G(j\omega)$ represents the plant frequency response. It is easy to understand that, if the direct chain delay is taken into account, than the limit condition of the stability is given by the *pseudo-characteristic equation*:

$$N(A) * G(j\omega) * e^{-j\omega\theta_a} = -1 \tag{2.15}$$

Equation (2.15) allows to determine the condition for which the process goes to the limit of stability, approaching the limit cycle oscillations. When this oscillation is held, the plant output signal is a permanent oscillation with fixed amplitude A_c and frequency $\omega_c = \frac{2\pi}{T_c}$. Than the magnitude and the phase of the system are therefore given by:

$$|G(j\omega_c)| = \frac{1}{|N(A_c)|} = \frac{A_c\pi}{4d} \tag{2.16}$$

$$\angle G(j\omega_c) = -\pi + \theta_a \omega_c \tag{2.17}$$

Equation (2.17) permits to easily change the oscillation frequency ω_c by acting on the delay θ_a to identify the process at different frequencies. Varying appropriately θ_a it is therefore possible to identify the system at the desired crossover frequency ω_{cg}. If, in the direct chain of the Fig. 2.6, the ideal relay is replaced with a relay with hysteresis, of $\pm x$ and $\pm d$ amplitude, the descriptive function results:

$$N(A) = \frac{4d}{\pi A} e^{-j \arcsin(\frac{x}{A})} \tag{2.18}$$

This approach lets to identify the process at a specific crossover frequency ω_{cg} given by the specifications of the control system. In order to determine the correct θ_a value, so that $\omega_c = \omega_{cg}$, the following iterative *Relay-test routine* has been implemented:

1) Two delays θ_{-1},θ_0 and the corresponding ω_{-1},ω_0 are fixed as the initial condition of the algorithm.
2) For n steps, the following iterative relation is applied:

$$\theta_n = \frac{\omega_{cg} - \omega_{n-1}}{\omega_{n-1} - \omega_{n-2}} (\theta_{n-1} - \theta_{n-2}) + \theta_{n-1} \tag{2.19}$$

3) If the current value of delay θ_n is negative, a zero is added into the forward chain and the procedure restarts from the beginning.
4) If the comparison between ω_c and ω_{cg} is close to zero (≈ 0.01) the procedure is stopped.

At the end of the iteration the identification of the process at the given frequency is obtained as:

$$G(j\omega_u) = |G(j\omega_u)|\, e^{j\angle G(j\omega_u)} \tag{2.20}$$

were ω_u is the real crossover frequency ($\omega_u \simeq \omega_{cg}$) and:

$$|G(j\omega_u)| = \frac{1}{N(A_n)} = \frac{A_n\pi}{4d} \tag{2.21a}$$

$$\angle(G(j\omega_u) = -\pi + \theta_a\omega_u \tag{2.21b}$$

One of the improvement given by this work is related to point 3), in fact the possibility to identify the process with an order greater than two has been ensured by adding a zero into the forward chain.

2.1.3 $PI^{\lambda}D^{\mu}$ Auto-tuning phase

From now on the $PI^{\lambda}D^{\mu}$ transfer function assumes the following form:

$$PI^{\lambda}D^{\mu}(s) = k_c x^{\mu} \left(\frac{\lambda_1 s + 1}{s}\right)^{\lambda} \left(\frac{\lambda_2 s + 1}{cs + 1}\right)^{\mu} \tag{2.22}$$

were it is possible to distinguish three different control actions, a *Proportional action*, a *Proportional-integrative action* and a *Proportional-derivative action*. The proportional one is assumed as $k_c x^{\mu} = N(A)x^{\mu} = 1$ to let the system be robust to gain variations.

Proportional-integrative action

The proportional-integrative action is obtained through the term:

$$PI^{\lambda}(s) = \left(\frac{\lambda_1 s + 1}{s}\right)^{\lambda} \tag{2.23}$$

This term is intended to flatten the phase of the system around ω_{cg} in order to obtain a system more robust to the gain variations. With this in view the phase slope ν close to ω_{cg} is computed by using the following relation:

$$\nu = \frac{\varphi_{n+1} - \varphi_{n-1}}{\omega_{n+1} - \omega_{n-1}} \tag{2.24}$$

where ω_{n-1} and φ_{n-1} are respectively the frequency and the phase at the $n-1$ iteration of the Relay-test. The delay θ_{n+1} at the $n+1$ iteration is evaluated via the following relation:

$$\theta_{n+1} = \theta_a + |\theta_a - \theta_{n-1}| \tag{2.25}$$

The phase of the $PI^{\lambda}(j\omega)$ block is given by:

$$\varphi\left(PI^{\lambda}(j\omega)\right) = -\lambda \arctan\left(\frac{1}{\lambda_1 \omega}\right) = \lambda\left(-\frac{\pi}{4} + \arctan(\lambda_1 \omega)\right) \tag{2.26}$$

and its derivative assumes the form:

$$\frac{d\left(\varphi\left(PI^{\lambda}(j\omega)\right)\right)}{d\omega} = \lambda\left(\frac{\lambda_1}{1 + (\lambda_1 \omega)^2}\right) \tag{2.27}$$

To obtain a flat phase slope, (2.27) must assume the opposite value of the slope given in (2.24) at $\omega = \omega_{cg}$, so it holds:

$$\lambda\left(\frac{\lambda_1}{1 + (\lambda_1 \omega_{cg})^2}\right) = -\nu \tag{2.28}$$

This relation depends both from λ and λ_1. In order to find both values, the first step is to derivate (2.26) with respect to λ_1 as it follows:

$$\frac{d\left(\varphi\left(PI^{\lambda}(j\omega)\right)\right)}{d\lambda_1} = \lambda \frac{1-(\lambda_1\omega_{cg})^2}{\left(1+(\lambda_1\omega_{cg})^2\right)^2}$$

To obtain that derivative equal to zero, the following condition must be granted:

$$1-(\lambda_1\omega_{cg})^2 = 0$$

that is satisfied if:

$$\lambda_1 = \frac{1}{\omega_{cg}} \tag{2.29}$$

From the (2.28) λ is calculated as:

$$\lambda = -\nu\left(\frac{1+(\lambda_1\omega_{cg})^2}{\lambda_1}\right) = -\nu\left(\frac{2}{\lambda_1}\right) \tag{2.30}$$

By fixing the previous obtained values of λ and λ_1 the proportional-integrative block has been designed and the following open loop transfer function

$$G_{flat}(s) = PI^{\lambda}(s) * G(s) \tag{2.31}$$

ensures a flat phase around the crossover frequency ω_{cg}.

Proportional-derivative action

After the set of the proportional-integrative action, to satisfy the phase margin φ_m and the crossover frequency ω_{cg} specifications it is used the term:

$$PD^{\mu}(s) = \left(\frac{\lambda_2 s + 1}{cs + 1}\right)^{\mu} \tag{2.32}$$

The block diagram after the proportional-integrative action is shown in Fig. 2.7

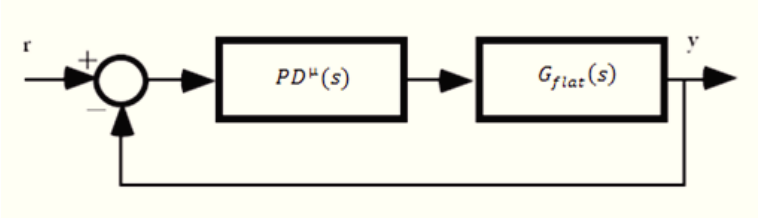

Fig. 2.7. PD^{μ} control block diagram.

The open loop transfer function is now:

$$F(s) = PD^{\mu}(s) * G_{flat}(s) \tag{2.33}$$

that, with $s = jw_{cg}$, assumes the form:

$$F(j\omega_{cg}) = e^{j(\varphi_m - \pi)} = \cos(\varphi_m - \pi) + j\sin(\varphi_m - \pi) \tag{2.34}$$

while for equation (2.31) it holds:

$$G_{flat}(j\omega_{cg}) = |G_{flat}(j\omega_{cg})| e^{j\varphi\left(G_{flat}(j\omega_{cg})\right)} =$$

$$= |G_{flat}(j\omega_{cg})| * (\cos(\varphi(G_{flat}(j\omega_{cg}))) + j\sin(\varphi(G_{flat}(j\omega_{cg})))) \tag{2.35}$$

Substituting (2.34) and (2.35) in (2.33), the following transfer function for $PD^{\mu}(j\omega_{cg})$ is obtained:

$$PD^{\mu}(j\omega_{cg}) = \left(\frac{\lambda_2 j\omega_{cg}+1}{x\lambda_2 j\omega_{cg}+1}\right)^{\mu} = \frac{F(j\omega_{cg})}{G_{flat}(j\omega_{cg})} = a_1 + jb_1 \tag{2.36}$$

where x takes into account of the high frequency pole added to guarantee the implementation of the controller, a_1 and b_1 are respectively the real and the imaginary part of the $PD^{\mu}(j\omega_u)$. Once a_1 and b_1 are determined, the module ρ and the phase ϕ are calculated by:

$$\rho = \sqrt{a_1^2 + b_1^2} \tag{2.37a}$$

$$\phi = tan^{-1}\frac{b_1}{a_1} \tag{2.37b}$$

Considering:

$$(a_1 + jb_1)^{\frac{1}{\mu}} = \rho^{\frac{1}{\mu}} * e^{j\frac{\Phi}{\mu}} = \rho^{\frac{1}{\mu}}\left(\cos\left(\frac{\Phi}{\mu}\right) + j\sin\left(\frac{\Phi}{\mu}\right)\right)$$

equation (2.36) can be rewritten as:

$$\left(\frac{\lambda_2 j\omega_{cg}+1}{x\lambda_2 j\omega_{cg}+1}\right) = (a_1 + jb_1)^{\frac{1}{\mu}} = a + jb \tag{2.38}$$

and then:

$$a = \rho^{\frac{1}{\mu}} * \cos\left(\frac{\Phi}{\mu}\right) \tag{2.39a}$$

$$b = \rho^{\frac{1}{\mu}} * \sin\left(\frac{\Phi}{\mu}\right) \tag{2.39b}$$

From the equation (2.38) the following conditions hold:

$$a = \left(\frac{x(\lambda_2\omega_{cg})^2+1}{(x\lambda_2\omega_{cg})^2+1}\right) \tag{2.40a}$$

$$b = \left(\frac{\lambda_2 \omega_{cg} - x\lambda_2 \omega_{cg}}{(x\lambda_2 \omega_{cg})^2 + 1} \right) \tag{2.40b}$$

$$\lambda_2 = \left(\frac{b^2 + a(a-1)}{b\omega_{cg}} \right) \tag{2.40c}$$

$$x = \left(\frac{a-1}{b^2 + a(a-1)} \right) \tag{2.40d}$$

By applying the below reported iterative algorithm it is possible to determine x, λ_2 and μ that represent the design parameters of (2.36).

1 μ is first fixed to a small value (ex. $\mu = 0.48$)
2 from the equation (2.39a) and (2.39b), a and b are calculated
3 from the equation (2.40c) and (2.40d), λ_2 and x are estimated
4 until $x > 0$, $a > 1$ e and $b > 0$, μ is iteratively incremented if $x \leq 0$ or $a \leq 1$ or $b \leq 0$ to obtain the minimum value μ_{min}
5 x and λ_2 are respectively estimated at μ_{min}

By adding the conditions $a > 1$ and $b > 1$, to the traditional one $x > 0$, and starting with $\mu > 0.48$ the algorithm converge recursively, being more efficient than the one proposed in [52].

2.1.4 Numerical Examples

In order to validate the procedures introduced in the previous section, the following three systems has been considered:

$$G_1(s) = \frac{0.55}{s(0.6s+1)} e^{-0.55s} \tag{2.41a}$$

$$G_2(s) = \frac{1}{s^2(2s+1)} \tag{2.41b}$$

$$G_3(s) = \frac{1}{s(2s+1)} \tag{2.41c}$$

$PI^{\lambda}D^{\mu}$ auto-tuning procedure for $G_1(s)$

The system $G_1(s)$ to be identified and controlled was characterized by the following Transfer Function:

$$G_1(s) = \frac{0.55}{s(0.6s+1)} e^{-0.55s} \tag{2.42}$$

As it can be noticed it presents three elements: a positive gain, two poles, one in $s = 0$ and one pole in $s = 1.667$ and a time delay. In this example the design specifications have been fixed as:

- $\omega_{cg} = 2.3 \frac{rad}{sec}$
- $\varphi_m = 60°$
- Gain variations robustness

In Fig. 2.8 the Bode Diagrams for the (2.41a) are shown.

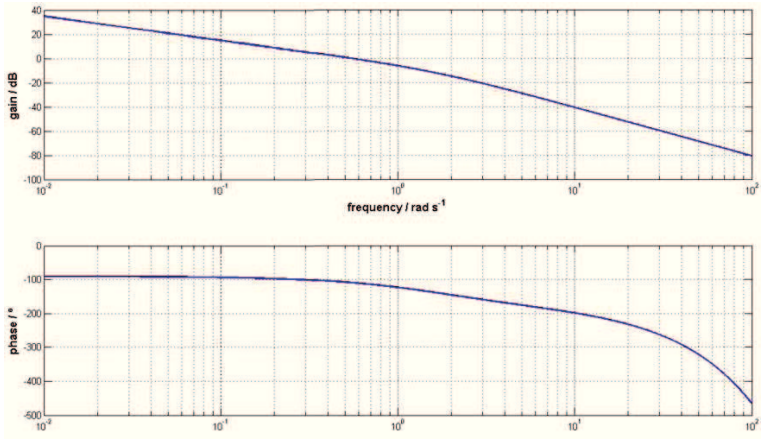

Fig. 2.8. $G_1(s)$ Bode Diagrams.

In Fig. 2.9 is reported the designed *Simulink* model for the Relay-test.

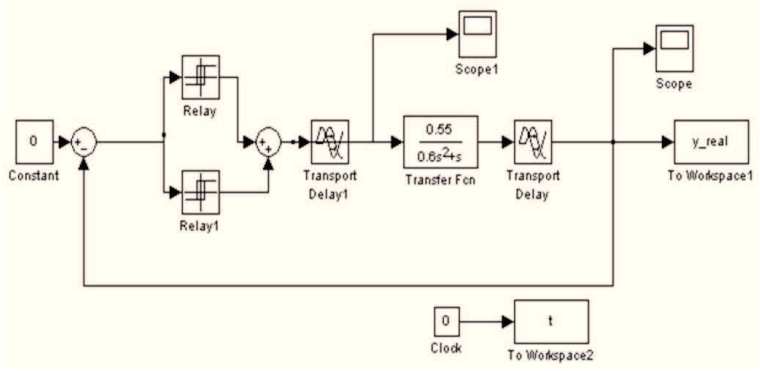

Fig. 2.9. $G_1(s)$ Simulink model for Relay-Test.

As it is shown, the following blocks were used:

- A null reference signal.
- Two ideal relays with output voltage equal to $|d| = 5V$ in symmetric working mode.
- Two delay, the first one to insert the θ_n iterative delay and the second one to apply the delay to the $G_1(s)$ Transfer Function.
- The $G_1(s)$ Transfer Function.
- Two workspaces to record the time and the output value arrays.

Following the iterative procedure described in the previous section, the first step was to apply the starting delay $\theta_{-1} = 0.05s$ to calculate ω_{-1} as:

$$\omega_{-1} = 3.7556\frac{rad}{s}$$

The same procedure is applied with $\theta_0 = 0.1s$ and ω_0 was obtained as:

$$\omega_0 = 3.0442\frac{rad}{s}$$

From the two coupled $(\omega_{-1}, \theta_{-1})$ and (ω_0, θ_0) the new delay $\theta_1 = 0.1523s$ was evaluated and applied to the *Simulink* block diagram to obtain the new θ_2 and so on. The iteration stopped when $|\omega_{cg} - \omega_n| \approx 0.01$ were obtained. As it is shown in Table 2.1 a good approximation were obtained at the 4^{th} iteration at which $\omega_u = 2.3015 \simeq \omega_{cg}$.

n	$\theta_n(s)$	$\omega_n \left(\frac{rad}{s}\right)$
-1	0.05	3.7556
0	0.1	3.0442
1	0.1523	2.5974
2	0.1871	2.3854
3	0.2011	2.3108
4	0.2031	2.3015

Table 2.1. $G_1(s)$ Relay-Test iterations.

After the Relay-test, the $PI^{\lambda}D^{\mu}$ modeling phase has began. The corresponding value $A_4 = 0.896V$ to the couple (ω_4, θ_4) was evaluated and given to the model to identify the Transfer Function module and phase at the desired frequency ω_u:

$$|G(j\omega_u)| = -17.0314dB \tag{2.43a}$$

$$\angle G(j\omega_u) = -153.1652^{\circ} \tag{2.43b}$$

To estimate the phase slope around ω_u a $\theta_{\mu-\delta} = 0.1631$ was applied and from the (2.25) the $\theta_{u+\delta} = 2.5269s$ was calculated. From

the *Simulink* model the corresponding values of $\omega_{u-\delta} = 2.5269\frac{rad}{s}$ and $\omega_{u+\delta} = 2.1217\frac{rad}{s}$ were calculated and applied in the (2.21b) to obtain the phases $\varphi(G(j\omega_{u-\delta})) = -2.7295rad$ and $\varphi(G(j\omega_{u+\delta})) = -2.6258rad$. From the (2.24) the phase slope $\mu = -0.2558$ was estimated and than the PI^{λ} parameters calculated ($\lambda_1 = 0.4345$ and $\lambda = 1.1774$). The PI^{λ} Transfer Function resulted:

$$PI^{\lambda} = \left(\frac{0.4345s + 1}{s}\right)^{1.1774} \tag{2.44}$$

In Fig. 2.10 the obtained Bode Diagrams are shown.

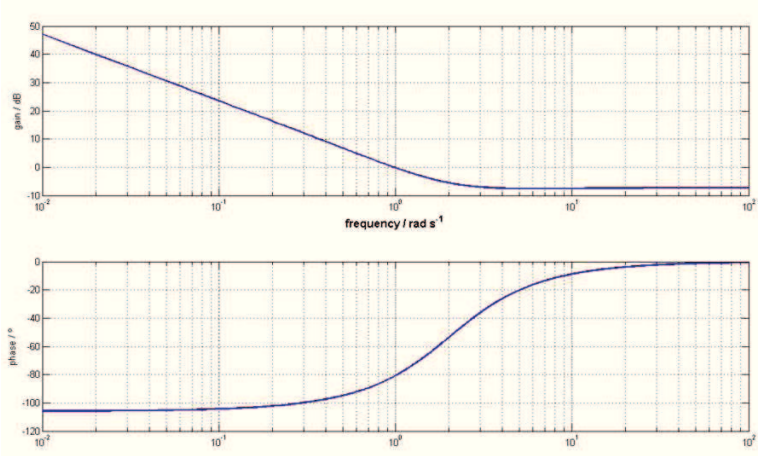

Fig. 2.10. PI^{λ} Bode Diagrams.

The open-loop system Transfer Function is obtained from the (2.31) with the following module and phase:

$$|G_{1flat}(j\omega_u)| = -23.2334dB$$

$$\angle G_{1flat}(j\omega_u) = -200.638^{\circ}$$

From the $G_{1flat}(j\omega_u)$ and imposing the phase margin $\varphi_m = 60°$ the PD^μ parameters has been calculated and obtained the following Transfer Function:

$$PD^\mu = \left(\frac{7.6985s + 1}{4.7137 * 10^{-4}s + 1}\right)^{0.93} \tag{2.46}$$

The corresponding Bode Diagrams are shown in Fig. 2.11.

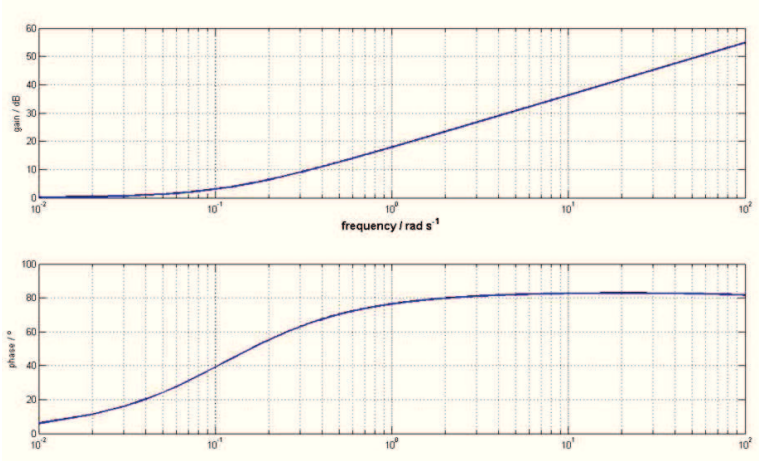

Fig. 2.11. PD^μ Bode Diagrams.

Applying the PI^λ and PD^μ Transfer Function founded, the project specifications for the open-loop control system were evaluated as follows:

$$|F(j\omega_u)| = 1.29dB$$

$$\angle F(j\omega_u) = -120.378°$$

$$\varphi_m = -120.378 + 180 = 59.622°$$

The related Bode Diagrams are shown in Fig. 2.12.

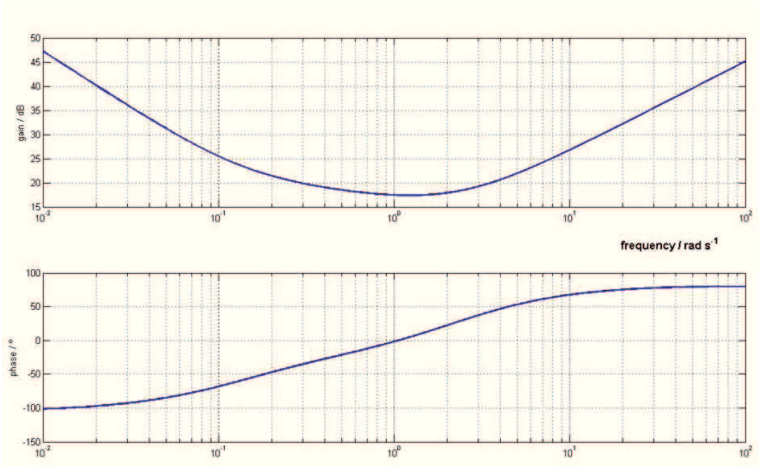

Fig. 2.12. Open-loop control system Bode Diagrams with $PI^{\lambda}D^{\mu}$.

Once the $PI^{\lambda}D^{\mu}$ controller was modeled, the step closed loop response was evaluated using the *Simulink* model shown in Fig. 2.13, in which the proportional (K_p), the non integer order integrative ($s^{-\lambda}$) and the non integer order derivative (s^{μ}) actions are shown.

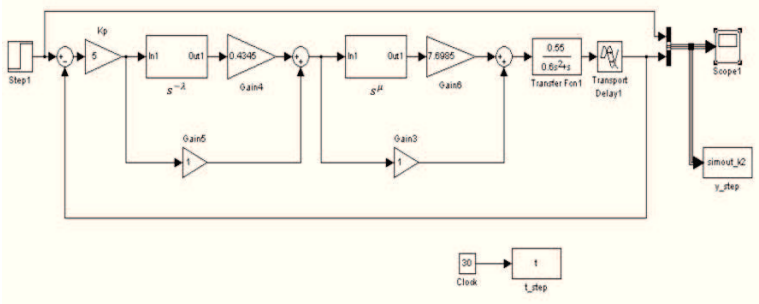

Fig. 2.13. Simulink block diagram of the controlled system.

The step response in shown in Fig. 2.14 in which the gain variation robustness is also shown.

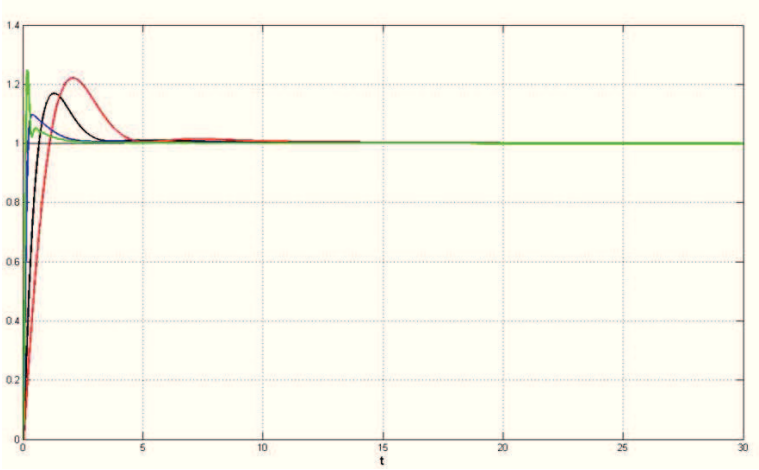

Fig. 2.14. Controlled system step response and gain variations ($K = 1$ in black, $K = 0.5$ in red, $K = 3$ in blue and $K = 6$ in green).

$PI^{\lambda}D^{\mu}$ auto-tuning procedure for $G_2(s)$

In the second example the following process Transfer Function was considered:

$$G_2(s) = \frac{1}{s^2(2s+1)} \tag{2.48}$$

The system to be identified and controlled, whose Bode Diagrams are shown in Fig. 2.15, was characterized by a unit gain, two poles in $s = 0$ and one pole in $s = 0.5$.

In this example the design specifications have been fixed as:

- $\omega_{cg} = 1.97 \frac{rad}{sec}$

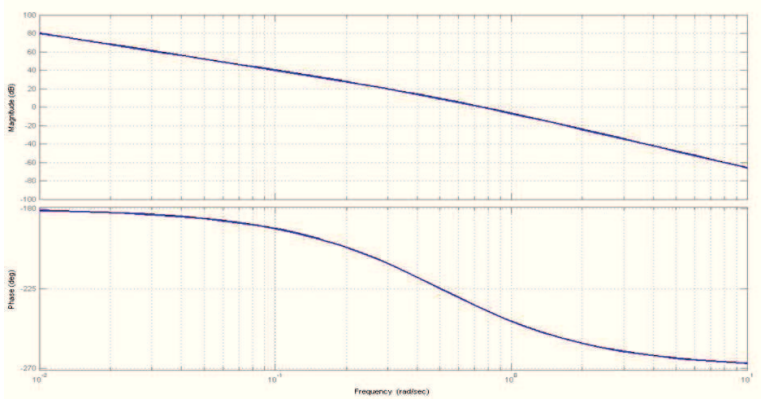

Fig. 2.15. $G_2(s)$ Bode Diagrams.

- $\varphi_m = 60°$
- Gain variations robustness

To start the relay-test routine, whose *Simulink* model is shown in Fig. 2.16, the relay output voltage was set to $|d| = 8V$ and the initial delay was fixed to $\theta_{-1} = 0.05s$ obtaining the first oscillating output signal y_{-1} for the closed loop system.

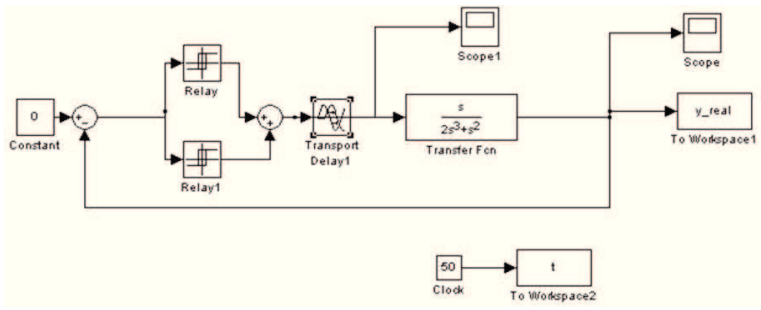

Fig. 2.16. $G_2(s)$ Simulink model for Relay-Test.

The amplitude, the period and the frequency of this output signal are computed obtaining $A_{-1} = 0.5753v$, $T_{-1} = 2.156s$ and $\omega_{-1} =$

$2.9143\frac{rad}{s}$. The same computation is done fixing a new $\theta_0 = 0.1s$ and obtaining $A_0 = 1.1322v, T_0 = 3.042s$ and $\omega_0 = 2.0655\frac{rad}{s}$. Starting from the evaluated couples (ω_{-1},θ_{-1}) and (ω_0,θ_0) and by applying equation (2.19), the new delay value $\theta_1 = 0.1056s$ is obtained. The relay-test iterative procedure has been stopped when $|\omega_{cg} - \omega_n| \approx 0.01$. The iteration results are shown in Table 2.2 where it possible to note that the desired cross-over frequency $\omega_u = 1.9727 \cong \omega_{cg}$ is reached at the fourth iteration.

n	$\theta_n(s)$	$\omega_n\left(\frac{rad}{s}\right)$
-1	0.05	2.9143
0	0.1	2.0655
1	0.1056	2.01
2	0.1096	1.9727

Table 2.2. $G_2(s)$ Relay-Test iterations.

As it can be noticed, the 2^{nd} iterations gave a good approximation obtaining $\omega_u = 1.9727 \simeq \omega_{cg}$. By substituting the value of the amplitude and the oscillation period, obtained at the final iteration ($A_2 = 1.2365V$ and $T_2 = 3.185s$), in equation (2.16) and (2.17) it was finally possible to determine the amplitude and the phase of the $G_2(s)$ at w_{cg}, that take respectively the values $|G(j\omega_{cg})| = -24.2173dB$ and $\varphi\left(G(j\omega_{cg})\right) = -257.6122°$, which are very close to the real values of $G_2(s)$. Once the module and the phase of $G(s)$ were determined at the cross-over frequency, the tuning phase of the $PI^{\lambda}D^{\mu}$ controller started. As in the previous example, the first control block that has been

considered was the integral one. To estimate the phase slope around ω_{cg}, a value of $\theta_{cg-\delta} = 0.08s$ was applied in equation (2.25) obtaining $\theta_{cg+\delta} = 0.1392s$ with the corresponding frequencies $\omega_{cg-\delta} = 2.3074\frac{rad}{s}$ and $\omega_{cg+\delta} = 1.7512\frac{rad}{s}$.

Then from equation (2.17) it was possible to determine the phases $\varphi\left(G(j\omega_{u-\delta})\right) = -2.957rad$ and $\varphi\left(G(j\omega_{u+\delta})\right) = -2.8978rad$. The phase slope $\nu = -0.1064$ was therefore obtained from the equation (2.24) and finally from equation (2.29) and (2.30), $\lambda_1 = 0.5069$ and $\lambda = 0.4198$ were determined so that the integral part of the fractional order controller was fixed:

$$PI^{\lambda}(s) = \left(\frac{0.5069s + 1}{s}\right)^{0.4198} \tag{2.49}$$

In Fig. 2.17 the Bode Diagrams for the PI^{λ} controller are shown.

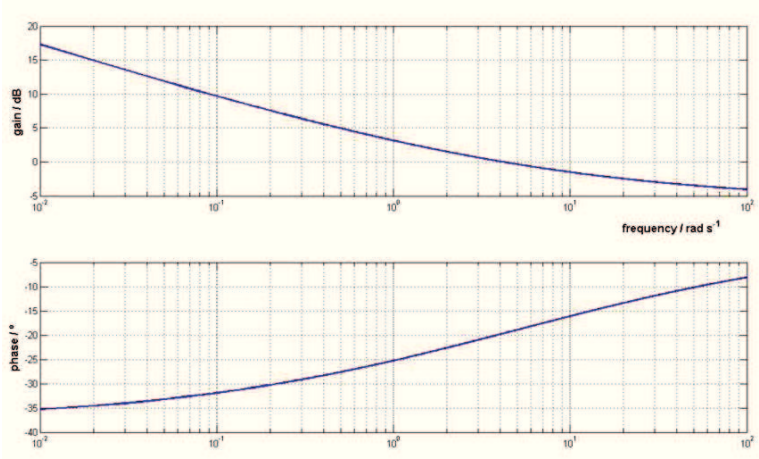

Fig. 2.17. PI^{λ} Bode Diagrams.

From equation (2.31) it was possible to compute $|G_{2flat}(j\omega_{cg})| = -25.4309dB$ and $\angle(G_{2flat}(j\omega_{cg})) = -276.5°$, showed also in Fig. 2.18.

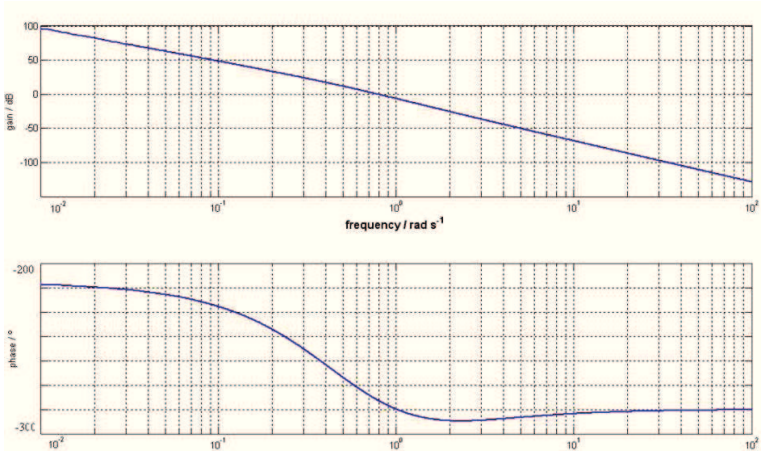

Fig. 2.18. $G_{1flat}(j\omega)$ Bode Diagrams.

The successive PD^{μ} tuning phase has been performed, as described previously, looking for a $\varphi_m = 60°$. According to the described procedure, the parameters $\mu = 1.826$, $x = 6.45 * 10^{-7}$, $\lambda_2 = 4.4251$ and $c = x * \lambda_2 = 2.8542 * 10^{-6}$ were determined so that the PD^{μ} block assumed the form:

$$PD^{\mu}(s) = \left(\frac{4.4251s + 1}{2.8542 * 10^{-6}s + 1}\right)^{1.826} \tag{2.50}$$

The module and phase of the open-loop control system Transfer Function were calculated as follow:

$$|F(j\omega_u)| = 0.4327dB$$

$$\angle F(j\omega_u) = -117.022°$$

$$\varphi_m = -117.022 + 180 = 62.978^\circ$$

In figure 2.19 the Bode Diagrams of the $PI^\lambda D^\mu(j\omega)$ controller is plotted.

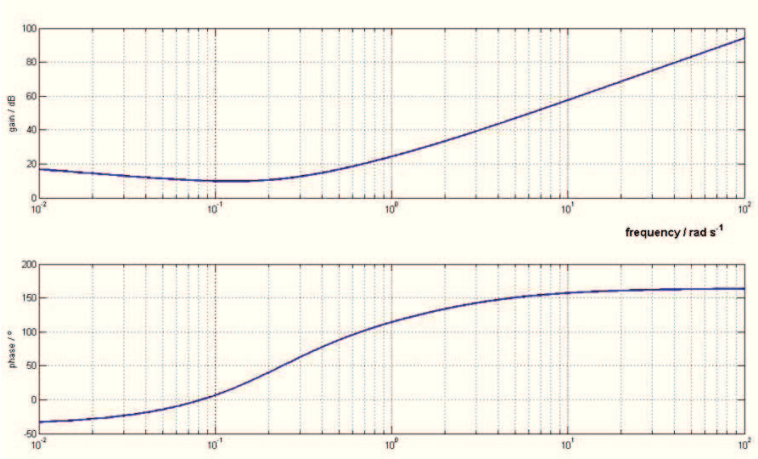

Fig. 2.19. $PI^\lambda D^\mu(j\omega)$ Bode Diagrams.

The *Simulink* model of the $PI^\lambda D^\mu$ controller is shown in figure 2.20, where the integro-differential equations of fractional order have been implemented according to the definition of Grunwald-Letnikov in [53]. By using this definition it is not necessary to approximate the fractional order PID controller with a transfer function of integer and high order so, as a consequence, the simulation results speed and without approximation.

The step responses of the controlled system are shown in figure 2.21, where it can be observed that the system exhibits robust performances to gain variations, keeping constant the overshoot of the time response.

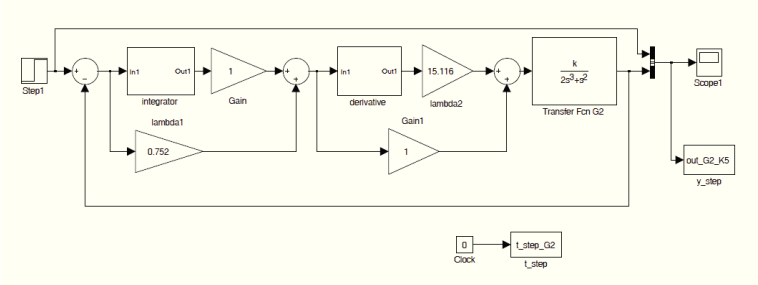

Fig. 2.20. Simulink block diagram of the controlled system.

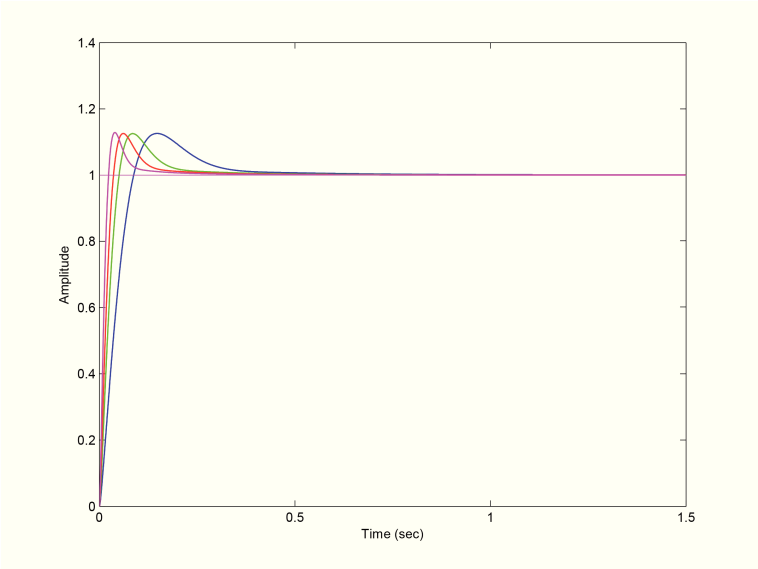

Fig. 2.21. Controlled system step response and gain variations ($K = 5$ in blue, $K = 10$ in green, $K = 15$ in red and $K = 25$ in magenta).

$PI^{\lambda}D^{\mu}$ auto-tuning procedure for $G_3(s)$

In the last example the following process Transfer Function was considered:

$$G_3(s) = \frac{1}{s(2s+1)} \tag{2.52}$$

It is relevant to outline that the proposed designed strategy has been implemented on an HIL (Hardware In the Loop) system, a *Dspace* board, while previous examples systems to be controlled have been simulated via their transfer function. Both the Relay-test and the $PI^{\lambda}D^{\mu}$ Auto-tuning have been in fact designed to be applied on real world system using the HIL approach. The system to be identified and controlled, whose Bode Diagrams are shown in Fig. 2.22, was characterized by a unit gain, one poles in $s = 0$ and one pole in $s = 0.5$.

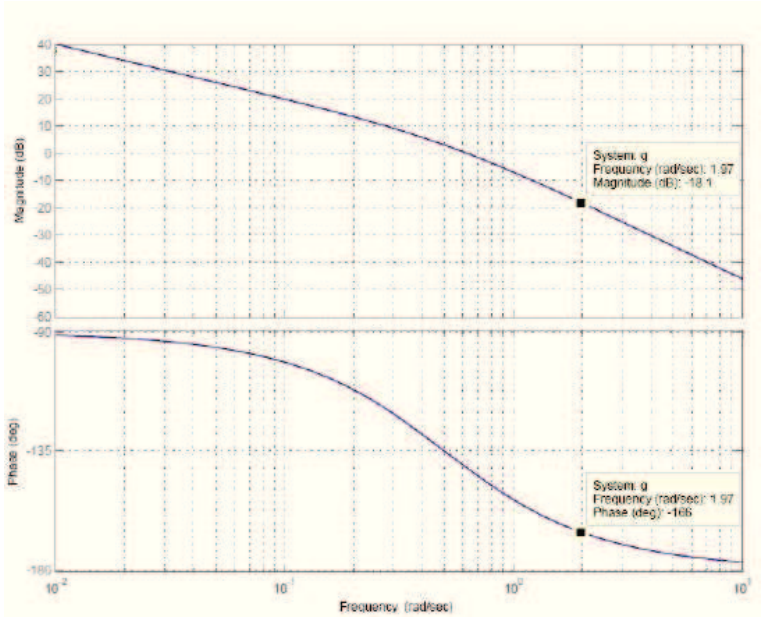

Fig. 2.22. $G_3(s)$ Bode Diagrams.

- $\omega_{cg} = 1.97 \frac{rad}{sec}$
- $\varphi_m = 60°$
- Gain variations robustness

Before designing the controller by using the HIL board, the system to be controlled has been realized in the circuit shown in Fig. 2.23, in which a TL082 Operational Amplifier, a $R = 10K\Omega$, a $R_L = 20K\Omega$, a $C = 100\mu F$ and a $C_L = 100\mu F$ were used.

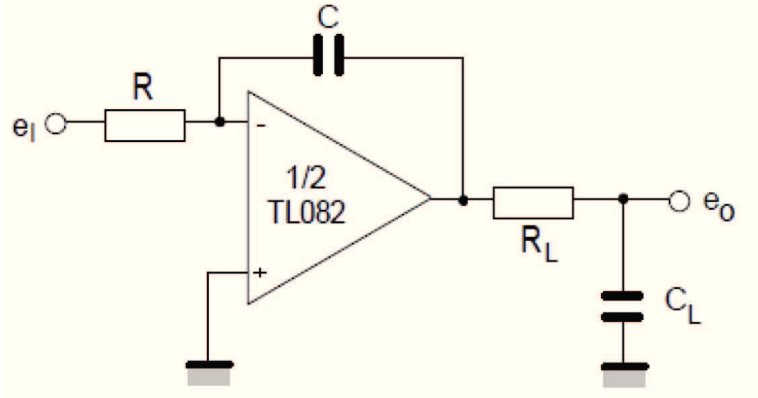

Fig. 2.23. OPAM implementation of the $G_3(s)$ system.

The implemented Transfer Function could be modeled as follow:

$$G(s) = \frac{e_o(s)}{e_i(s)} = \frac{1}{-RCs(R_L C_L s + 1)} \tag{2.53}$$

In Fig. 2.24 the adopted experimental setup, in which the design and synthesis of the $PI^{\lambda}D^{\mu}$ controller is realized by using the dSPACE board connected to the plant, previously realized on a breadboard, is shown.

The relay-test routine has been implemented through the *Simulink* model shown in Fig. 2.25 in which it is possible to note that the plant was interfaced to the dSPACE system through internal ADC and DAC converters.

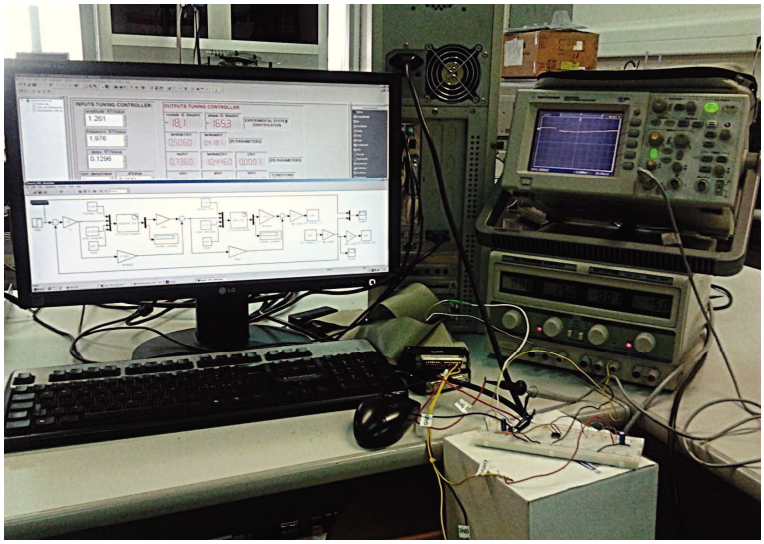

Fig. 2.24. Experimental setup.

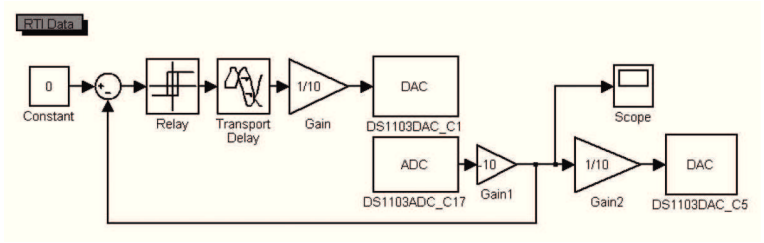

Fig. 2.25. RTI relay-test block diagram.

In order to identify the system at the desired crossover frequency, acting in real-time on the delay θ_a, a graphic interface, shown in Fig. 2.26 has been developed by using the *ControlDesk* environment.

The output signal, used during the design phase, is shown in Fig. 2.27. It is possible to note that the amplitude $A_c = 1.261V$ and the desired cross-over frequency $\omega_u = 1.9761\frac{rad}{sec} \cong \omega_{cg}$ were reached with the delay $\theta_a = 0.1296s$ and the relay output $|d| = 8V$.

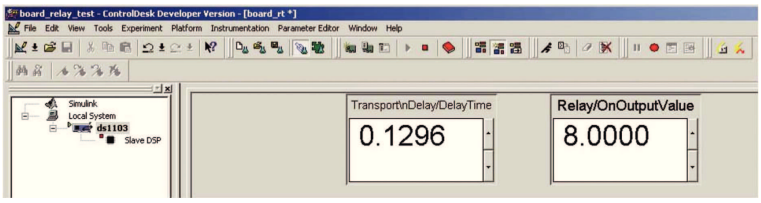

Fig. 2.26. Relay-Test routine in ControlDesk.

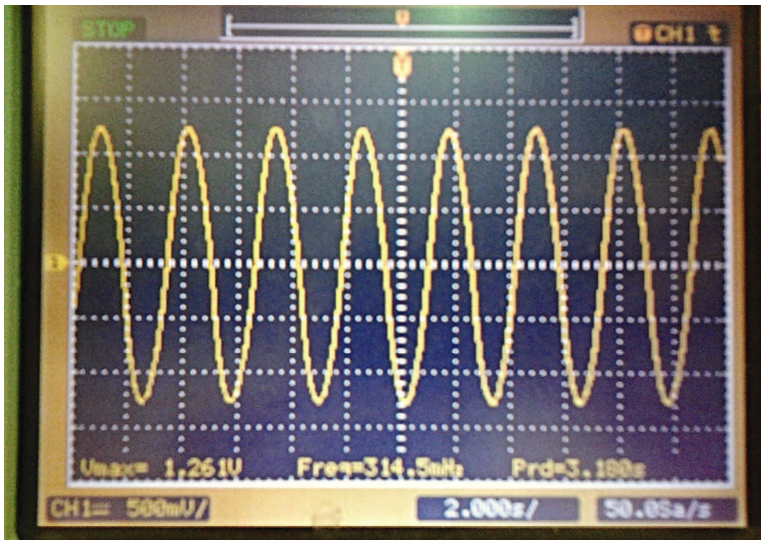

Fig. 2.27. Output signal of the Relay-test.

By substituting these values in equations (2.16) and (2.17) it was finally possible to determine the magnitude and the phase of the system, respectively $|G_3(j\omega_{cg})| = -18.15dB$ and $\varphi\left(G_3(j\omega_{cg})\right) = -165.3°$, that resulted very close to the real values. Once the module and the phase of experimental system were determined, the tuning phase of the $PI^{\lambda}D^{\mu}$ controller started. To estimate the phase slope around ω_{cg}, a value of $\theta_{cg-\delta} = 0.0796s$ was applied in equation (2.25) obtaining $\theta_{cg+\delta} = 0.1796s$, where the corresponding frequencies are $\omega_{cg-\delta} = 2.575\frac{rad}{s}$ and $\omega_{cg+\delta} = 1.671\frac{rad}{s}$ respectively. From equation

(2.17) the phases $\varphi\left(j\omega_{cg-\delta}\right) = -2.937rad$ and $\varphi\left(j\omega_{cg+\delta}\right) = -2.841rad$ were determined and then the corresponding phase slope $\nu = -0.1058$ was obtained from equation (2.24).

The $PI^{\lambda}D^{\mu}$ Auto-tuning procedure has been implemented trough the $sfuntion$ blocks in a *Simulink* model shown in Fig. 2.28. It possible to see that the parameters have been determined so that the $PI^{\lambda}D^{\mu}(s)$ controller assumed the form:

$$PI^{\lambda}D^{\mu}(s) = \left(\frac{0.506s+1}{s}\right)^{0.4181}\left(\frac{10.446s+1}{0.0007s+1}\right)^{0.736} \tag{2.54}$$

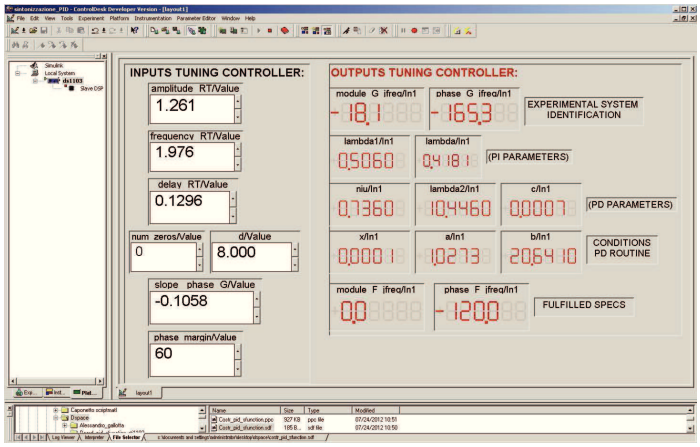

Fig. 2.28. $PI^{\lambda}D^{\mu}$ auto-tuning procedure in ControlDesk on dSPACE system.

The *Simulink* model of the $PI^{\lambda}D^{\mu}$ controller is shown in Fig. 2.29. The integro-differential equations of fractional order have been implemented according to the definition of Grunwald-Letnikov as in [20].

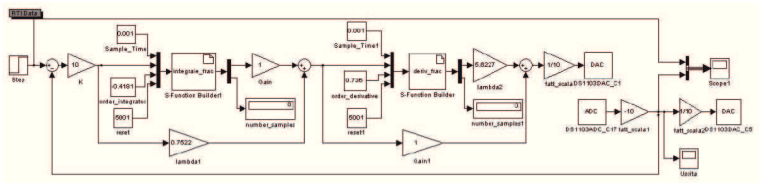

Fig. 2.29. RTI block diagram of the fractional experimental system for different gain values.

The *CaptureSettings* instrument is added in the ControlDesk project for the acquisition of the step responses while varying the open loop gain K. The step responses of the controlled system are shown in Fig. 2.30. It is possible to observe that the system exhibits robust performances to gain variations, keeping constant the overshoot of the step responses.

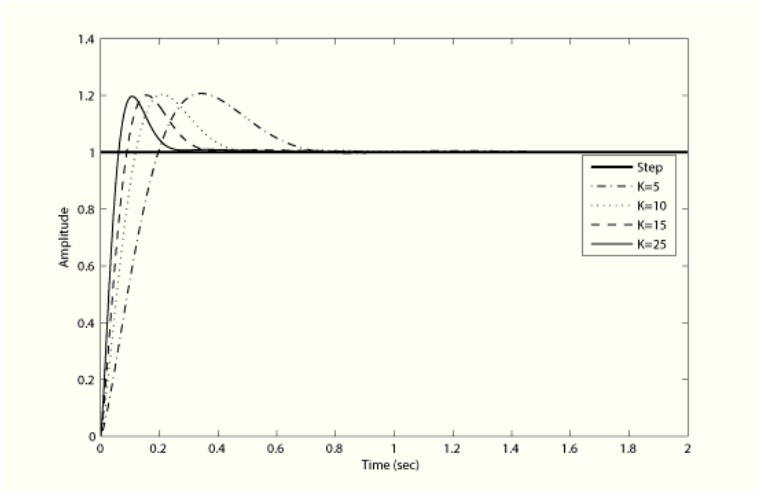

Fig. 2.30. Step responses with different gain values.

3

Fractional Order Elements: Modeling and Realization

This chapter is focused on the modeling and realization of fractional order elements. In the first and second sections a brief introduction on Electro Active Polymers and Ionic Polymer Metal Composite (*IPMC*) is presented. In the third section a novel class of composite materials (*IPMC*) capable of electromechanical reversible transduction are presented. They can be modeled by fractional Transfer Function and for that reason a grey box approach to identify IPMC actuators is proposed. Moreover the proposed Transfer Functions are ruled by using the device geometrical parameters in such a way to guarantee the control of the transducer during the design phase: after a theoretical discussion on experimental validation of the proposed approach is reported. In the fourth section a study on characterization of IPMC as Fractional Order Elements (*FOE*) is presented. The goal is to define a fabrication procedure that allows to realize a FOE with the desired non integer order characteristics. This element is proposed as the

basic building block of Fractional Order Controllers realization.

3.1 Introduction on Electro Active Polymers

New applications in a number of interesting fields, such as of bio inspired robotics, active prostheses, smart textiles, artificial tissues and organs and novel sensors, just to mention a few, will be possible, in the near future, largely because of new polymeric materials that are becoming available thanks to strongly interdisciplinary research activities including material sciences, engineering, mechanics, and biology. These new materials are able to sense external stimuli and react to them, e.g. by changing their shape, so that they are not anymore passive tools but will be capable to cooperate to reach our objectives. A key role in the deep changes described above is played by Electro Active Polymers (*EAPs*), i.e. polymers that exhibit a mechanical reaction to an electrical stimulus and viceversa. EAPs could be divided in two different classes: *Dry-EAP*, which are characterized by a deformation caused by the local distribution of the electric field, fast dynamics, but need high voltage supply and *Wet-EAP* in which the deformation is linked to the ionic diffusion. This last class of EAPs presents a low voltage supply activation, but lower dynamics and strength density [54]. The interest on EAPs is quite recent, it is dated to the end of last century and it raised partly as the consequence of the discovery of some electroactive materials that are capable to undergo deformations larger that 100% , offering electromechanical properties that cannot be obtained by classes of competitive materials. They are also generally light and flexible so that are known as artificial muscles. The capability of

EAPs to react to electrical inputs with significant mechanical changes makes them suitable candidates to be used as mechanical actuators. It has been also shown that for a lot of EAPs electromechanical transduction phenomena are reversible, so that one technology could be used both to realize actuators and sensors paving the road to obtain smart materials that incorporate both capabilities [55]. Among EAPs, during the last two decades, Ionic Polymer Metal Composites (*IPMCs*) have been extensively studied, due to a number of promising characteristics, including the possibility to obtain very large deformations as reaction to a voltage signal of few volts. IPMCs belongs to the class of ionic EAPs, since transduction phenomena are due to ionic motion or ionic diffusion. Also, they need a solvent, generally water, to work properly. It is generally accepted that one of the main drawbacks of IPMC based actuator is represented by the large dependence on their response of factors such as fabrication process, water content and temperature [56]. As a result IPMCs can not be used in open loop schemes and control strategies are needed to improve IPMC based applications [57], [58], [59]. Controlling strategies require the knowledge of models to be used in the design of the IPMC controller. Moreover such models should be scaled as a function parameters that are under designer that can fix those parameters in order to obtain the desired system performance [60]. It has been reported that IPMCs have a fractal electrode structure [61] and that non integer transfer functions can be used to describe their transduction properties [62]. IPMCs consist of a layer of ionic polymer, whose thickness is generally of the order of $100\mu m$, inter-

posed between two conductive layers, to realize the electrodes. Nobile metals, such as platinum or gold, are used to this purpose. Electrodes are used both to impose the electrical stimulus when an IPMC is used as an electromechanical transducer, and to collect electrical signals, when the IPMC is used as a sensor. The polymer most widely used is Nafion, a perfluorinated alkene produced by DuPont [63]. Since Nafion shares with Teflon its antiadherent electrodes cannot be simply applied to the polymer and a chemical plantation procedure need to be used. Following the standard impregnation reduction procedure proposed by Dr. Oguro [64], a sheet of $Nafion^{®}117$, whose thickness was about $180\mu m$, was first allowed to soak in a platimun salt solution, typically $PtNH3Cl2$. As the second step the membrane was soaked in a reducing agent, allowing metallic dendritic structure to build into the ion exchange membrane and to realize the electrodes at the membrane surface. It is generally accepted that such dentritic structure plays a main role in the electromechanical coupling behavior of the IPMC transducer since it contributes in largely increase the effective area of the electrodes. Also the dentritic nature of the electrodes suggested the fractional order modeling of IPMCs [65], [66]. The electrodes realized by using the procedure described so far are quite thin and since the thickness of electrodes contribute to reduce the electrode resistance (ideal electrode are supposed to be perfect conductor) a secondary plating process has been implemented. As a result of the production steps, a sample soaked in water and whose thickness was about $200\mu m$ was obtained. This has been further cut to obtain the transducers with the

desired shape, i.e. rectangular strips with different length and width. Different theories have been proposed to explain the electromechanical transduction properties of IPMCs. More specifically, Tadokoro and Yamagami proposed, in their paper (citeTadokoro), that the actuation mechanism is due to the migration of mobile ions under the effect of the external electric field. Moreover, Nafion is among the most hydrophilic materials counter ions carry parasitically a number of water molecules so that this part of the membrane expands while the opposite occurs at the anode region and the IPMC bands. The transduction phenomenon has been also explained by considering the electrostatic interactions within the polymer [68]. The stress according to Nemat-Nasser is due to electrostatic forces that generate because of the interaction between ions. For the case of the IPMCs used as sensors the deformation pushes the solvent and mobile ions so that an electric signal can be collected at the electrodes. A mature technology should produce devices for the solution of applications, in new fields and/or with performances that cannot be obtained by using competing technologies. The evolution of a technology requires the comprehension of relevant phenomena. This phase requires the experimental investigation of the new devices and the modeling of their behavior, with relevant efforts. The product of this phase is mathematical models, that with an adequate level of accuracy, describe the behavior of the novel devices. This allows the user to predict the effects of his choices during the design step of new devices. Models can be generally classified into:

- *Black Box Models*, that approximate the behavior of a device under test by using solely experimental data without any attempt to describe the underlying mechanisms. Also, they lack any generalization capability and are of little or no utility for devices different from that used for the model identification [69], [70].
- *White Box Models*, that try to describe the observed behavior of devices by the comprehension of the phenomena involved in the transduction process. They have opposite pros and cons with respect to black box models, since they are very hard to be investigated, depending on parameters that cannot be directly observed, and, generally are inaccurate so that might be not very useful for the designer [71], [68].
- *Gray Box Models*, that represent a useful compromise between the competing requirements of simplicity, accuracy and generality. They are obtained on the basis of some well understood theories and use parameters that can be experimentally determined. Moreover parameters can be used that depend only on the characteristic of the materials, so that the model can be scaled on the basis of the geometry size of the device under test or under design [72], [60], [73].

IPMCs are generally considered as a pinned beam and the Eulero Bernoulli theory is used for modeling. The transduction phenomena are then modeled by using suitable coupling terms in a similar way as for the case of piezoelectric devices [74]. In that paper is also shown the necessity to model the Young modulus a complex function of the input signal. The same holds true for the electromechanical coupling

term that assumes the form of a complex function of the applied signal frequency.

3.1.1 IPMC Structure, Working Principles and Manufactoring

IPMCs are based on a polymer containing ions, also called ionic polymers, that are weakly linked to the polymer chain and metallized via a chemical process, on both sides, with a noble metal, to realize the electrodes. There are a number of different types of ionic polymers available but the typical IPMC used in many investigations is composed of a perfluorinated ion-exchange membrane, $Nafion^{®}117$, which is surface-composite by platinum via chemical process (Fig. 3.1.

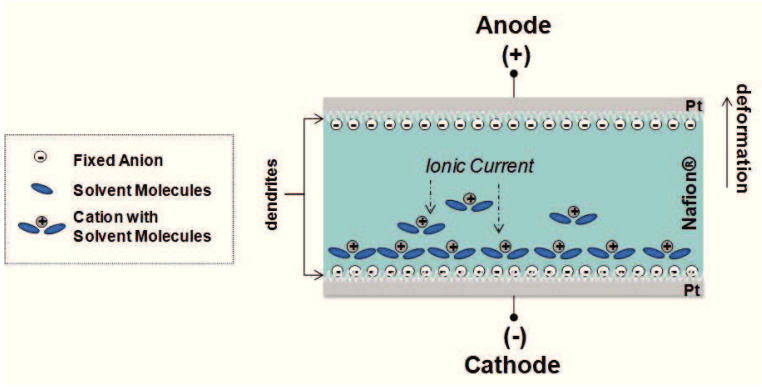

Fig. 3.1. Structure and Working Principle of IPMC.

The Platinum electrodes often consist of small, interconnected metal particles which are made to penetrate into the ionic polymer membrane. This results in the formation of electrodes with dendritic structures [62],

[75] which extend from the surface into the membrane. Working as an actuator, when an external voltage is applied across the thickness of the IPMC, mobile cations (H^+) in the polymer will move toward the cathode. Moreover, if a solvent is present in the sample, the cations will carry solvent molecules with them. The cathode area will expand while the anode area will shrink. If the tip of the IPMC strip is free the polymer will bend toward the anode; thus a force will be delivered. On the other hand, when the IPMC works as a sensor, it exploits the mechanical displacement of the polymer for the generation of a ionic current inducing a potential difference. In general the relationship between the applied potential and absorbed current will be affected by the ionic current and the solvent flow within the sample and by the interaction of the ions and the solvent molecules with the polymer/metal interface. The devices described in this section are made of a $Nafion^{®}117$ films with thickness $t_{Naf} = 180\mu m$ and sizes $4x4cm$ that was pre-treated by successive boiling for $30min$ in HCl_2N and deionized water. Ethylene glycol (EG) was used as the solvents and Platinum as the electrodes. Two platinum metallization were obtained by immersion of the $Nafion^{®}117$ membrane in a solution of $P_t(NH_3)_4Cl_2$ with molecular weight equal to $M_w = 334.12$. This immersion time is here referred to as *Absorption time*. The platinum solution was obtained by dissolving $205mg$ of the complex in $60ml$ of deionized water and adding $1ml$ of ammonium hydroxide at 5%. In order to increase the performance of the device, a dispersing agent (Polyvinylpyrrolidone with molecular weight $M_w = 10000$) has been added. Moreover, a secondary metal-

lization was performed via deposition. Then the samples were boiled in $0.1M$ of HCl for $1h$. In order to obtain the IPMC with EG as solvent, $Nafion^{®}117$ membranes were soaked overnight in a beaker containing pure EG and, finally, heated to $60 \circ C$ for $1h$.

3.2 Modeling phase and Parametric Control of Fractional Order IPMC Actuator

IPMC actuators suffer because of a large number of influencing factors that do not allow adequate open loop working conditions and they require the use of controlling strategies. IPMC controllers can be designed by using suitable device models. Here a non integer order transfer function is used to model IPMC actuators [76], [77], [78], [79]. In the present section the IPMC model is scaled as a function of the actuator length and the control law has been parameterized according to this physical parameter. When a voltage signal is applied across the thickness of the IPMC, mobile cations will move toward the cathode. Moreover the cations will carry solvent molecules with them with a resulting bending of the membrane.

3.2.1 Experimental Setup

Considering the beam parameters, the length L_{free} and the cross-sectional dimensions with thickness t and width w, it will be assumed that the beam vibrates in the vertical plane. The experimental setup, shown in Fig. 3.2, was composed of an *Agilent Technologies 33220A*

20MHz signal generator to impose the voltage input signal to the membrane, a *Baumer Electrics OADM12U6430* distance laser sensor to measure the tip deflection and a *National Intruments I/O* board for data acquisition. A picture of the implemented setup is shown in Fig. 3.3.

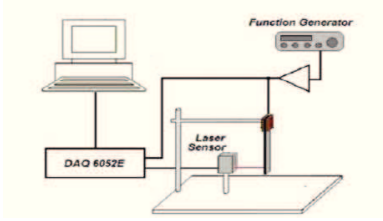

Fig. 3.2. Scheme of experimental setup.

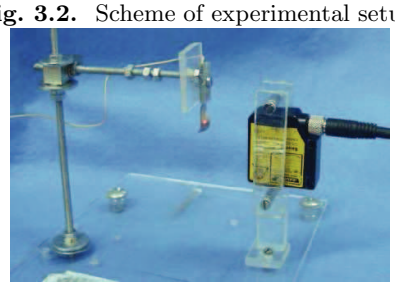

Fig. 3.3. Experimental setup picture.

Light from the laser diode was focused onto the end of the cantilever and the absorbed current was transduced by using a shunt resistor. As an example the voltage input imposed to the membrane and the deflection of the cantilever tip are shown respectively in Fig. 3.4(a) and 3.4(b), respectively.

The voltage input signal was a chirp signal with $3V_{pp}$ amplitude spanning from $500mHz$ to $100Hz$. Using a sampling frequency equal

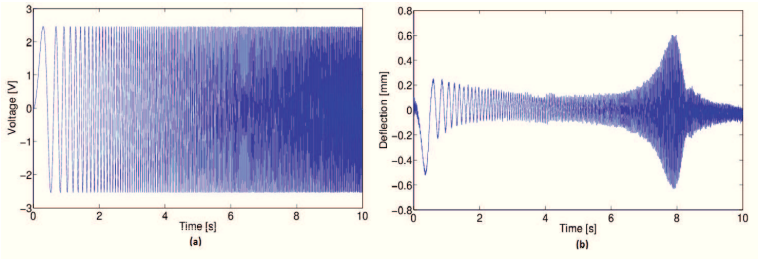

Fig. 3.4. Voltage input applied to the membrane (a), Deflection of the cantilever tip measured with the laser sensor (b).

to $1000 samples/s$, 10000 samples were obtained for a data acquisition campaign lasting $10s$. The output signal acquired, the deflection of the cantilever tip, showed clearly that the IPMC reaches the maximum deflection in the resonance condition. Processing these data in Matlab Environment, the transfer functions voltage-current, current-deflection and voltage-deflection have been obtained, supposing that the system was linear, using the *tfestimate* Matlab function. In Fig. 3.5 the voltage-deflection transfer functions, for three different length values of the membrane are shown.

The frequency analysis of the IPMC behavior was limited to the frequency range of $0.5 - 100Hz$ because this was the range on which IPMCs work as actuators. By the inspection of Bode diagrams it is easy to note that the three systems present a non integer order behavior [80], in fact the module of the Bode diagrams presents a slope equal to $\pm m * 20db/decade$, and the phase Bode diagrams present a phase lag equal to $\pm m * 90°$, where m is a suitable real number. The system can therefore identified by fractional order models which allows to obtain good modeling performance by using a small set of parame-

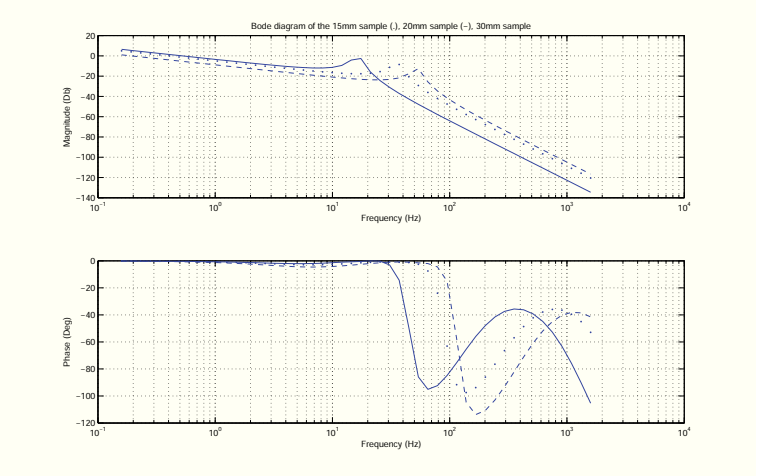

Fig. 3.5. Module and phase of three IPMC samples with different length.

ters [60],[62]. The fractional order models of the system has been determined by using the Marquardt algorithm [81] to the available data. The Levenberg-Marquardt method is commonly used to solve nonlinear least squares problems that have to be faced when fitting a parameterized function to a set of measured data by minimizing the sum of the squares of the errors between the data points and the function. The Levenberg-Marquardt curve-fitting method is actually a combination of two minimization methods: the gradient descent method and the Gauss-Newton method. It is similar to a gradient-descent method when the parameters are far from their optimal value, and acts more like the Gauss-Newton method when the parameters are close to their optimal value.

3.2.2 Modeling Phase

The models obtained for the voltage-deflection transfer function, have been determined according to the following relation:

$$G(s) = \frac{k}{s^n(s^2 + 2s\alpha + \alpha^2 + \beta^2)^m} \tag{3.1}$$

with $n = 0.62$ and $m = 1.15$. An analysis on the IPMC beams was performed taking into account six membranes of different length, from $15mm$ to $30mm$. In particular the Bode Diagrams of the membranes of $15mm$, $20mm$ and $30mm$ are shown in Fig. 3.6.

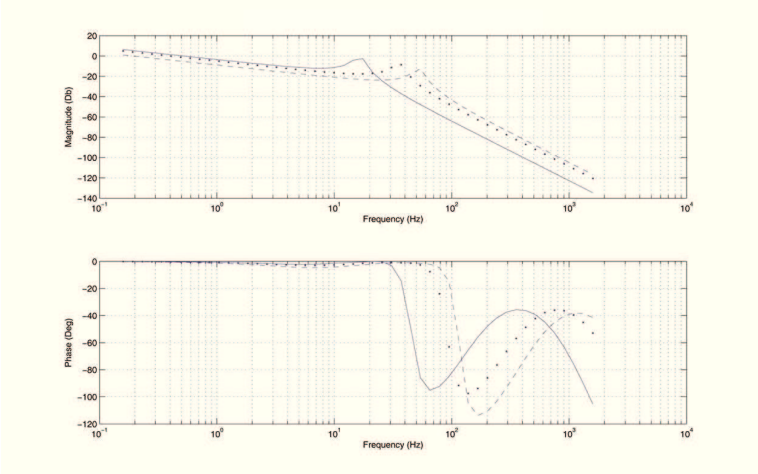

Fig. 3.6. Module and phase of three IPMC samples of $30mm$, $15mm$ (.) and $20mm$(-) of length.

In order to perform the IPMC control system design the resonance frequency as been parameterized (3.2) as a function of the membrane length, so that the parametric controller can be designed.

$$f_r = 0.09L^2 - 6.4L + 130 \tag{3.2}$$

Parameter α and β depends of the IPMC membranes length as reported in Table 3.1.

$L(mm)$	$f_r(Hz)$	α	β
15	53.86	26	330
18	41.50	25	262
20	35.36	20	223
25	24.31	10	153
27	21	10	133
30	16.36	7	103

Table 3.1. Model parameters according to the sample length.

The relationship between α, β and the length L of the membrane has been fixed through the following first order equation, accordingly to the interpolation shown in Fig. 3.7:

$$\alpha = -1.34L + 45.9 \tag{3.3a}$$

$$\beta = -15.02L + 540.2 \tag{3.3b}$$

In Table 3.2 are reported the real values of α and β and their estimations obtain by using the linear approximation in (3.3a) and (3.3b) respectively.

From the (3.1 it is also possible to parameterize the resonant frequency with respect to α and β obtaining the following relations:

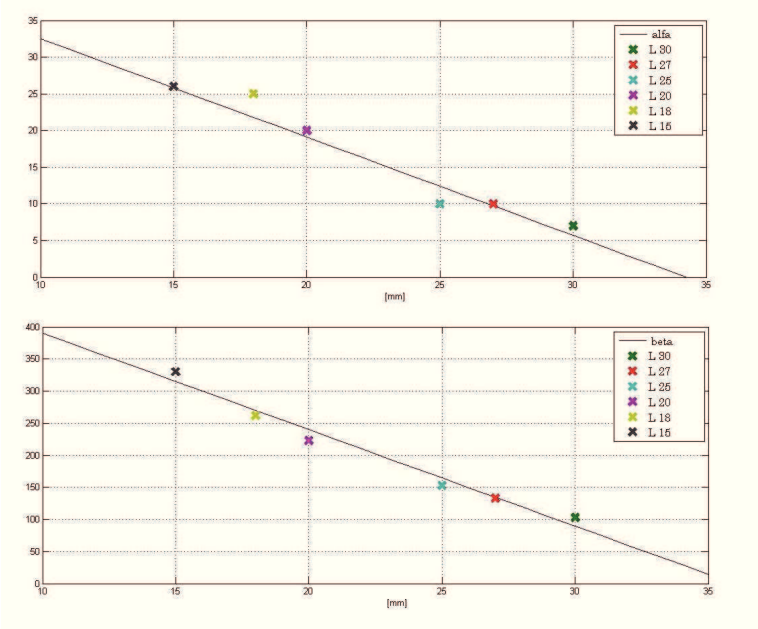

Fig. 3.7. Linear interpolation of $\alpha(L)$ and $\beta(L)$.

	Experimental data			1^{st} *order model*		
$L(mm)$	$f_r(Hz)$	α	β	$f_r(Hz)$	α	β
15	53.86	26	330	50	25.8	314.9
18	41.50	25	262	42.82	21.78	269.8
20	35.36	20	223	38.06	19.1	239.8
25	24.31	10	153	26.15	12.4	164.7
27	21	10	133	21.39	9.72	134.7
30	16.36	7	103	14.24	5.2	89.6

Table 3.2. Comparison between IPMCs acuator parameters and corresponding estimation.

$$\alpha = \xi\omega_n \tag{3.4a}$$

$$\beta = \omega_n\sqrt{1+\xi^2} \tag{3.4b}$$

3.2.3 Parameterized control of the membrane

Starting from the non integer order IPMC model (3.1), a parametric controller, depending on the membrane length L has been designed. The goal of the control system was to stabilize the closed loop system, to enlarge the bandwidth and to ensure a good tracking error. As it is shown in Fig. 3.8, the controller was characterized by the presence of three blocks: $C(s) = C_a(s)C_b(s)C_c(s)$.

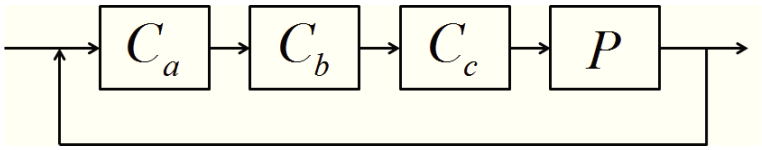

Fig. 3.8. Control scheme block diagram.

Each part of the controller had a different role:

- $C_a(s)$ has been added in order to guarantee a finite error to the step input. It consists in a zero with slope 0.62 and in a gain that has been fixed during a trial and error procedure.

$$C_a(s) = 33s^{0.62} \tag{3.5}$$

item $C_b(s)$ is the parameterized block and has been added to obtain a good phase margin at the desired crossover frequency.

$$C_b(s) = \frac{(1+s\tau)^3}{(1+s\frac{\tau}{m})^3} \tag{3.6}$$

where $m = 10$ and

$$\tau = \frac{0.5}{(2\pi f_r * 3.5)}$$

- $C_c(s)$ has been designed to guarantee a good tracking error inside the desired band width.

$$C_c(s) = \frac{(1+\frac{s}{16\pi})}{(1+\frac{s}{2\pi})} \tag{3.7}$$

The obtained open loop and closed loop transfer functions Bode Diagrams are reported in Fig. 3.9 and 3.10 respectively, in which it can be observed that a crossover frequency greater than $50Hz$ has been obtained for any membrane length, corresponding to a bandwidth greater than $80Hz$. Regarding the phase margin the worst case ($M_\phi = 20°$) and the best one ($M_\phi = 80°$) have been obtained for the $15mm$ and $30mm$ membrane length respectively..

3.3 Experimental characterization of novel Fractional Order Elements

As introduced in the previous section, Ionic Polymer Metal Composites (IPMCs) are electroactive materials made of ionic polymer thin membranes with Platinum metallization on their surfaces. They are interesting materials due to, besides their electromechanical applications as transducers, also to their electro-chemical features and to the

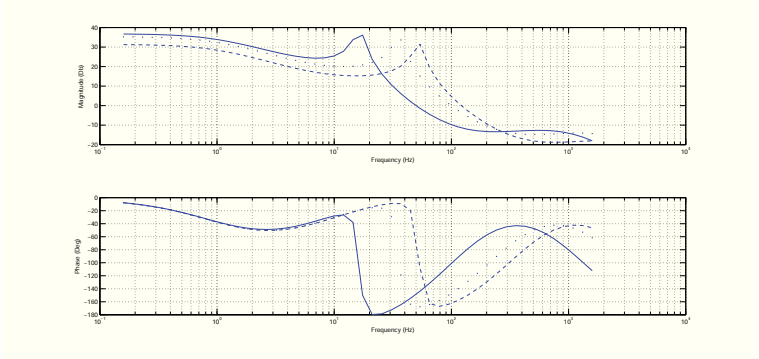

Fig. 3.9. Bode Diagrams of the open loop control system.

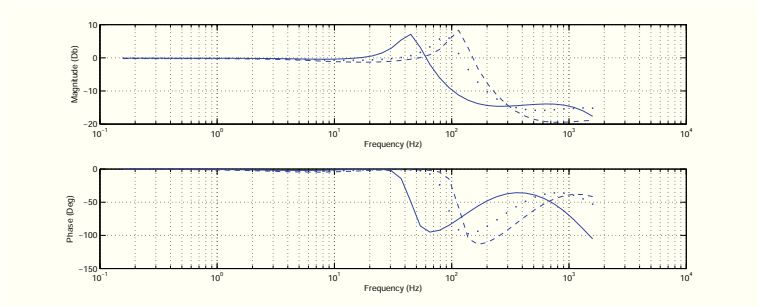

Fig. 3.10. Bode Diagrams of the closed loop control system.

relationship between the ionic/solvent current and the potential field. Their electro-chemical properties thus suggest the possibility for exploiting them as compact Fractional Order Elements (FOEs) with a view to defining fabrication processes and production strategies that assure the desired performances. In this section the experimental electrical characterization of a brand new FOE setup in a fixed sandwich configuration is proposed. Two different characterization through experimental data are here presented:

- FOE devices with different Platinum absorption times ($5h$, $20h$) [82]

- FOE devices with different *Polyvinylpyrrolidone* dispersing agent concentrations ($0.0005mol$, $0.001mol$, $0.002mol$) [83]

First, a preliminary linearity study was performed for a fixed input voltage amplitude in order to determine the frequency region where the FOE can be approximated as linear, then a frequency analysis was carried out in order to identify a coherent fractional order dynamics in the Bode diagrams. Such analysis take the first steps towards a simplified model of IPMC as a compact electronic FOE for which the fractional exponent value depends on fabrication parameters as the absorption time and the dispersing agent concentration. From the manufactory process described in Section 3.1.1, the obtained IPMC was cut into strips of size $1x1cm$ and dried for one week. Some IPMC sample are shown in Fig. 3.11.

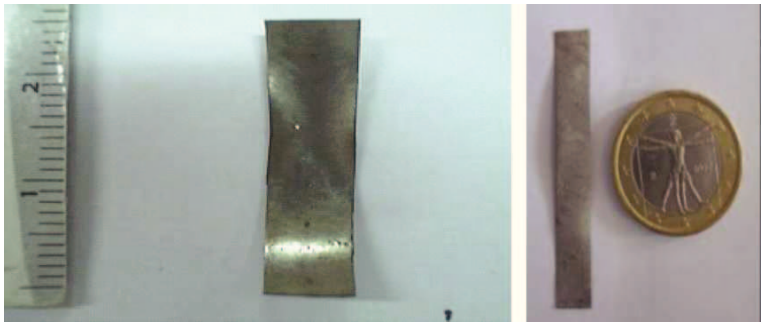

Fig. 3.11. IPMC samples.

3.3.1 FOE devices with different Platinum absorption times

Two different IPMC membranes have been fabricated with different absorption times, $5h$ and $20h$ in order to study the relationship between such a fabrication parameter and the fractional order dynamics of the FOE device. The two membranes will be here referred to respectively as FOE_{5h} and FOE_{20h}. The new FOE device here proposed consists of an IPMC strip of $1x1cm$ mechanically fixed within a Plexiglas sandwich configuration in series with a resistor with $R = 46\Omega$ as shown in the schematic in Fig. 3.12. The input voltage signal (V_{in}) was driven by a waveform generator (*Agilent 33220A*) through a conditioning circuit made of an operational amplifies in buffer configuration (*ST TL082CP*). The output voltage (V_{out}) was measured through a pair of copper electrodes ($1x1cm$ and thickness $35\mu m$) printed on a PBC board and in direct contact with the entire platinum electrodes.

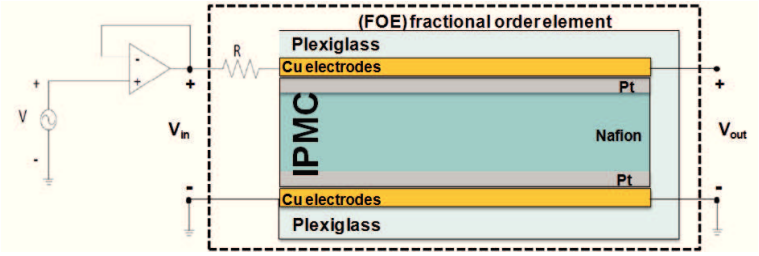

Fig. 3.12. FOE sandwich configuration schematic.

Both the input V_{in} and output V_{out} signals were acquired by using a National Instrument (*NI USB-6251*) board and processed by the

$LabView^{®}$ software. A schematic of the experimental setup is reported in Fig. 3.13.

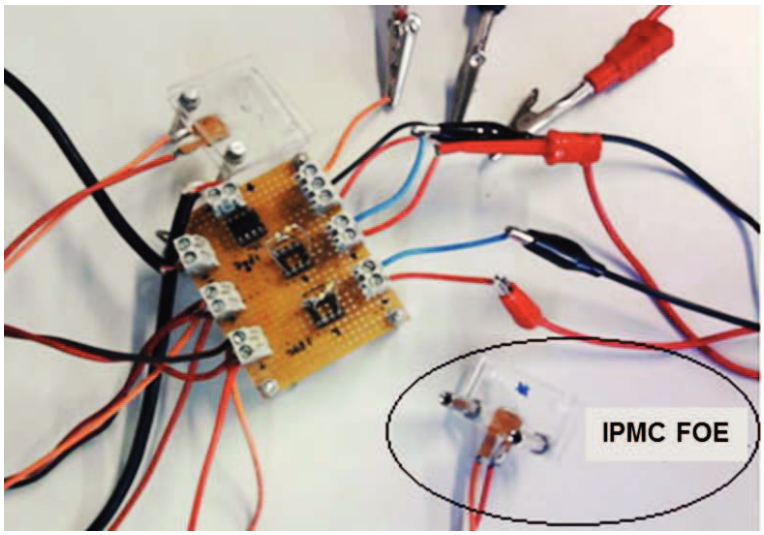

Fig. 3.13. IPMC FOE Experimental setup.

A preliminary linearity analysis based on experimental data has been performed in order to determine the frequency band where the FOE device can be approximated as linear. Under the linearity hypothesis a frequency domain characterization approach was performed. It has been based on the Bode Diagrams of the Transfer Function obtained by the ratio between the output (V_{out}) and the input (V_{in}) voltage in the frequency domain:

$$G(s) = \frac{V_{out}(s)}{V_{in}(s)} \tag{3.8}$$

Measurements have been performed on the two membranes FOE_{5h} and $FOE20h$. A set of sine voltages with amplitude of $4V_{pp}$ was ap-

plied as input and the output voltage was measured. For each membrane different measures were performer varying V_{in} frequency in the range from $10mHz$ to $10kHz$ with $10Hz$ step. Matlab^{TM}tools were then used to estimate the modulus and phase of the acquired signals. As literature has shown how IPMC membranes working as transducers present a nonlinear component in the electro-mechanical model and show an hysteretic behavior in the relationship between applied voltage and absorbed current [60] the hypothesis of linearity must be verified in this work in order to consider the frequency response as a coherent characterization for IPMC. Moreover, being the system nonlinear, such characterization is valid only for the given input voltage amplitude ($4V_{pp}$). Lissajous curves have been therefore studied in order to characterize the linearity of the IPMC as FOE. A Lissajous curve was obtained at each frequency for the complete experimental range for both FOE_{5h} and FOE_{20h}. Fig. 3.14, Fig. 3.15, Fig. 3.16 and Fig. 3.17 show such curves for the device FOE_{5h}.

Moreover Fig. 3.18 shows zoomed curves for sample frequencies of $50mHz$, $1Hz$, $9Hz$ and $4kHz$. It is worth noticing that at low frequencies the nonlinear component dominates and the Lissajous curves have a non-elliptic shape. In particular under the $1Hz$ frequency the curves show nonlinearity, while $1Hz$ is a frequency of transition from nonlinearity to linearity. For frequencies higher than $1Hz$ the Lissajous curves' shape can be considered elliptic. The FOE_{20h} shows the same trend in the Lissajous curves, therefore the same conclusion about linearity has been extended to it.

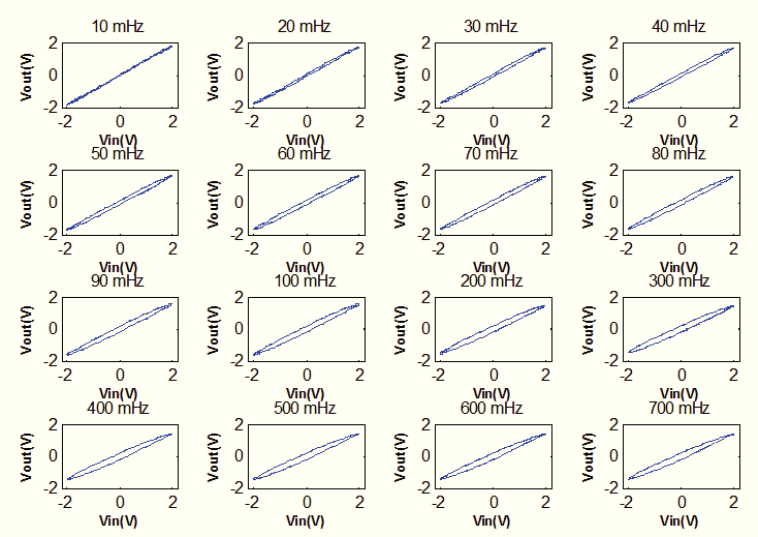

Fig. 3.14. FOE_{5h} Lissajous curves on measured V_{in} and V_{out} voltages in the frequency range between $10mHz$ to $700mHz$.

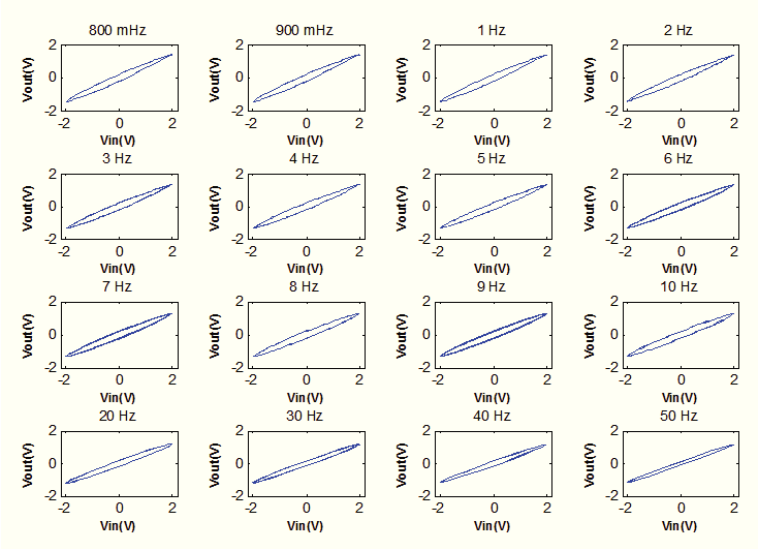

Fig. 3.15. FOE_{5h} Lissajous curves on measured V_{in} and V_{out} voltages in the frequency range between $800mHz$ to $50Hz$.

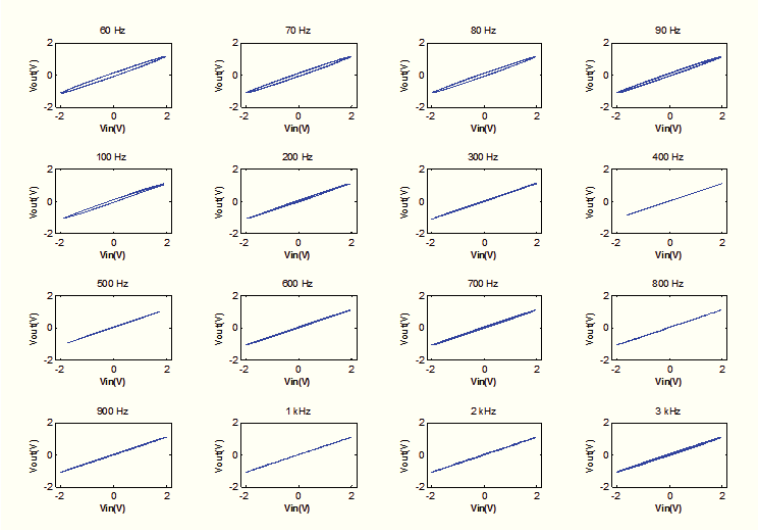

Fig. 3.16. FOE_{5h} Lissajous curves on measured V_{in} and V_{out} voltages in the frequency range between $60Hz$ to $3kHz$.

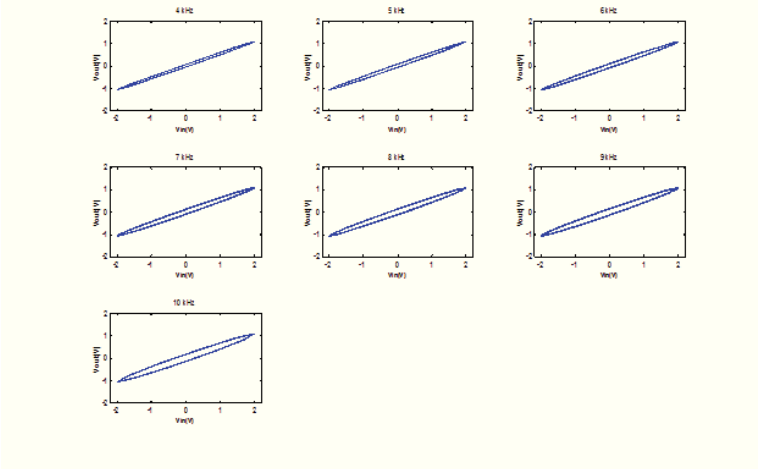

Fig. 3.17. FOE_{5h} Lissajous curves on measured V_{in} and V_{out} voltages in the frequency range between $4kHz$ to $10kHz$.

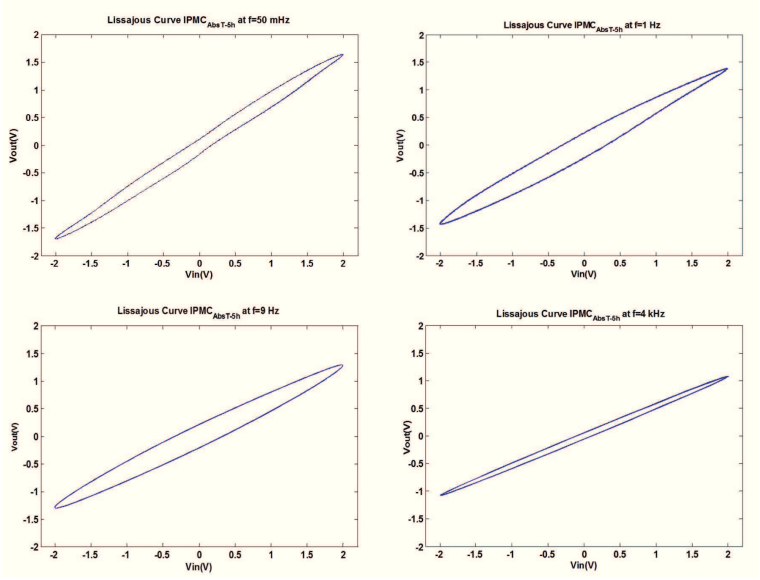

Fig. 3.18. Shape analysis of FOE_{5h} Lissajous curves on measured V_{in} and V_{out} at $50mHz$ (top-left), transition between non-elliptic to elliptic shape at $1Hz$ (top-right), elliptic shape at $9Hz$ (bottom-left) and $4kHz$ (bottom-right).

Such considerations are confirmed by literature [60], where the IPMC model as transducer is represented by a nonlinear component connected to capacitive elements. At low frequencies the capacitance are considered open circuits and the nonlinearity dominates the global behavior. As the frequency increases the linear capacitive effect of IPMC becomes significant and dominant with respect to the nonlinear component. For that reasons the FOE device has been approximated as linear in a frequency range from $1Hz$ to $10kHz$. Given the conclusion on linearity assessed by the Lissajous plots, the Bode Diagrams of the (3.8) at each frequency have been obtained by using the experimental data in the frequencies range between $10mHz$ to $10kHz$ for

both the devices FOE_{5h} and FOE_{20h} in the linearity range from $1Hz$ to $10kHz$. In such a range, it was observed that both FOE devices show a fractional order behavior, here identified with α, in a limited span of frequencies where the Bode Diagrams present a module slope of $\alpha * 20\frac{dB}{dec}$ and a phase lag of $\alpha * 90°$ both depending on the $\alpha \in \Re$ fractional order exponent. In the specific, in the frequency range between $1Hz$ to $100Hz$:

- FOE_{5h} has shown an average slope in the module diagram of $1\frac{dB}{dec}$, determining $\alpha = 0.05$. The phase diagram showed an average phase of $-4.5°$ being coherent with the fractional exponent related to the modules $-\alpha * 90° = -4.5°$.
- FOE_{20h} showed an average slope in the module diagram of $6\frac{dB}{dec}$, determining $\alpha = 0.3$. The phase diagram showed an average phase of $-27°$ showing coherence with the fractional exponent related to the modules $-\alpha * 90° = 27°$.

In Fig. 3.19 and 3.20 the Module and Phase Diagrams of the 3.8 of the FOE_{5h} and FOE_{20h} respectively are shown.

In Fig. 3.21 the linear approximation, expressed by the (3.9), of the relationship between the fractional order exponent of the IPMC system (α) and the variation of the absorption time (h) is shown.

$$\alpha = 0.0066h + 0.03 \tag{3.9}$$

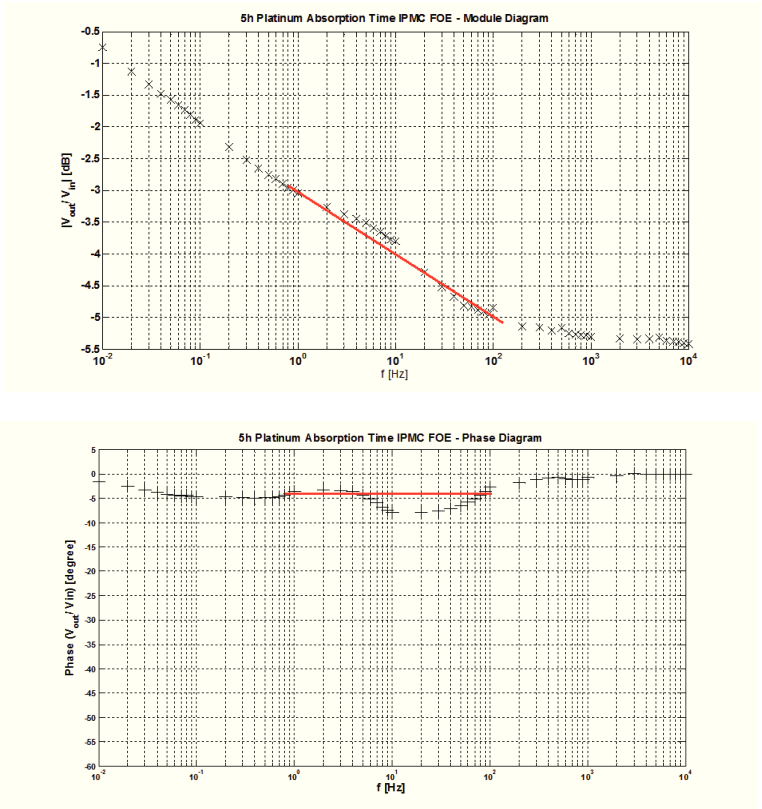

Fig. 3.19. FOE_{5h} Module and Phase Diagrams in frequencies range from $10mHz$ to $10kHz$.

3.3.2 FOE devices with different Polyvinylpyrrolidone dispersing agent concentrations

As introduced in previous sections, during the IPMCs manufactory process, in order to increase the device performances, a dispersing agent (*Polyvinylpyrrolidone* - PVP) is added. Considering this, three different FOE membranes have been fabricated with different PVP concentrations, $0.0005mol$, $0.001mol$ and $0.002mol$ in order to study the relationship between such a fabrication parameter and the fractional order

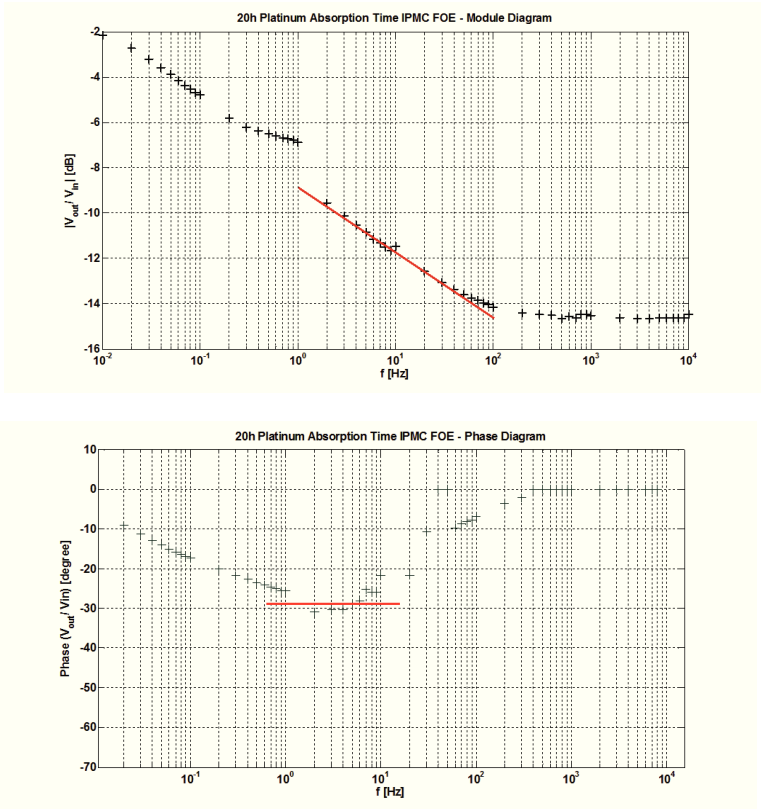

Fig. 3.20. FOE_{20h} Module and Phase Diagrams in frequencies range from $10mHz$ to $10kHz$.

dynamics of the FOE device itself. The membranes will be here referred to respectively as $FOE_{0.0005}$, $FOE_{0.001}$ and $FOE_{0.002}$. The same circuit used to characterize the FOE_{5h} and FOE_{20h} has been used in this study and the membranes strip of $1x1cm$ were mechanically fixed within a Plexiglas sandwich configuration as it is shown in Fig. 3.13. The input voltage signal ($V_{in} = 4V_{pp}$) was driven by the *Agilent 33220A* waveform generator and the output voltage (V_{out}) was measured through a pair of copper electrodes ($1x1cm$ and thickness $35\mu m$)

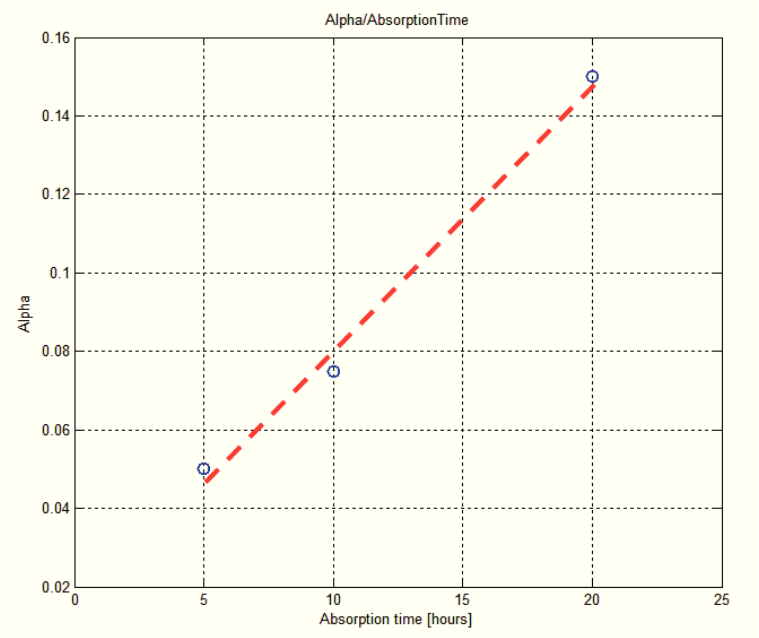

Fig. 3.21. Linea approximation of α referred to absorption time variation.

printed on a PBC board and in direct contact with the entire platinum electrodes. Both the input V_{in} and output V_{out} signals were acquired by using a National Instrument (*NI USB-6251*) board and processed by the $LabView^{®}$ software. A preliminary linearity analysis based on experimental data has been performed in order to determine the frequency band where the FOE device can be approximated as linear. Under the linearity hypothesis a frequency domain characterization approach was performed. It has been based on the Bode Diagrams of the Transfer Function obtained by the ratio between the output (V_{out}) and the input (V_{in}) voltage in the frequency domain. Measurements have been performed on the three membranes $FOE_{0.0005}$, $FOE_{0.001}$ and $FOE_{0.002}$. A set of sine voltages with amplitude of $4V_{pp}$ was applied as

input and the output voltage was measured. For each membrane different measures were performer varying V_{in} frequency in the range from $100mHz$ to $9kHz$ with $a100^b$ step were $a = 1, 2, ..., 9$ and $b = 0, 1, ..., 5$ so to evaluate the logarithm plots in each point of the five decades. The (3.8) Bode Diagrams, obtained by using the experimental data in the frequencies range between $100mHz$ to $9kHz$, of the three devices are shown in Fig. 3.22.

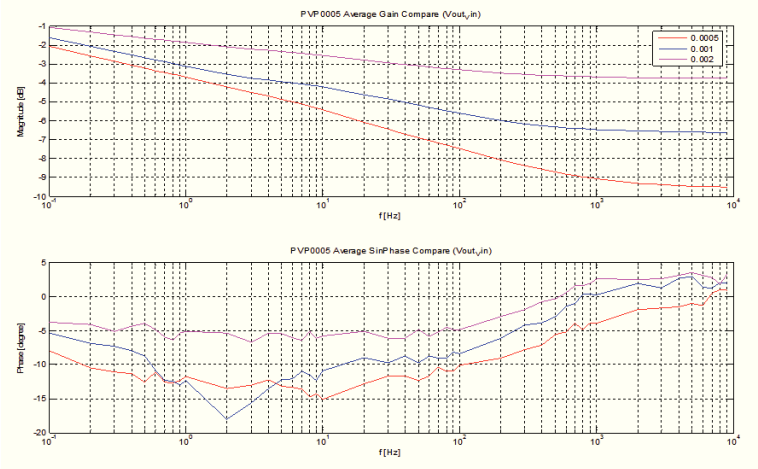

Fig. 3.22. Bode Diagrams of $FOE_{0.0005}$ (red), $FOE_{0.001}$ (blue) and $FOE_{0.002}$ (magenta).

As it was noticed by the plot analysis, the linearity range was assumed in the decade from $10Hz$ to $90Hz$. Moreover, being the system nonlinear, such characterization is valid only for the given input voltage amplitude ($4V_{pp}$). Lissajous curves have been therefore studied in order to characterize the linearity of the IPMC as FOE. A Lissajous curve was obtained at each frequency for the complete experimental range for both $FOE_{0.0005}$, $FOE_{0.001}$ and $FOE_{0.002}$ devices. Fig. 3.23,

Fig. 3.24 and Fig. 3.25 show such curves for the devices $FOE_{0.0005}$, $FOE_{0.001}$ and $FOE_{0.002}$ respectively highlighting the linearity behavior (green circle) in that frequency range.

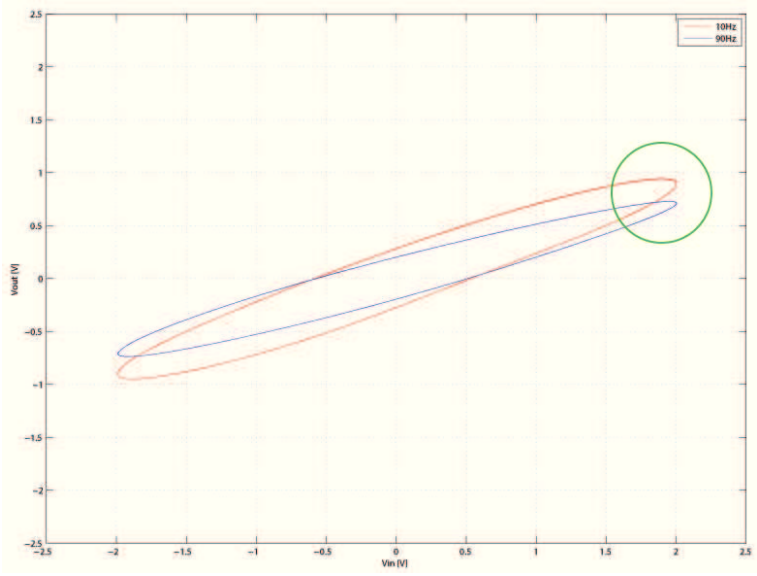

Fig. 3.23. $FOE_{0.0005}$ Lissajous curves on measured V_{in} and V_{out} voltages at frequency $10Hz$ (purple) and $90Hz$ (blue).

In such a range, it was observed that both FOE devices show a fractional order behavior in a limited span of frequencies where the Bode Diagrams present a module slope of $m * 20\frac{dB}{dec}$ and a phase lag of $m * 90°$ both depending on the $m \in \Re$ fractional order exponent. This exponent was evaluated both for modules and phase Diagrams and a singular consideration has been made: these devices presented a different fractional order exponent for the two characteristics (module

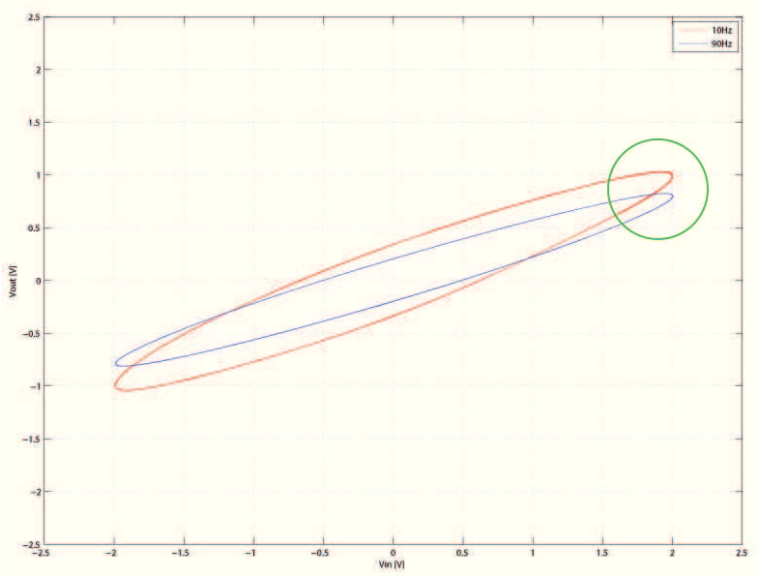

Fig. 3.24. $FOE_{0.001}$ Lissajous curves on measured V_{in} and V_{out} voltages at frequency $10Hz$ (purple) and $90Hz$ (blue).

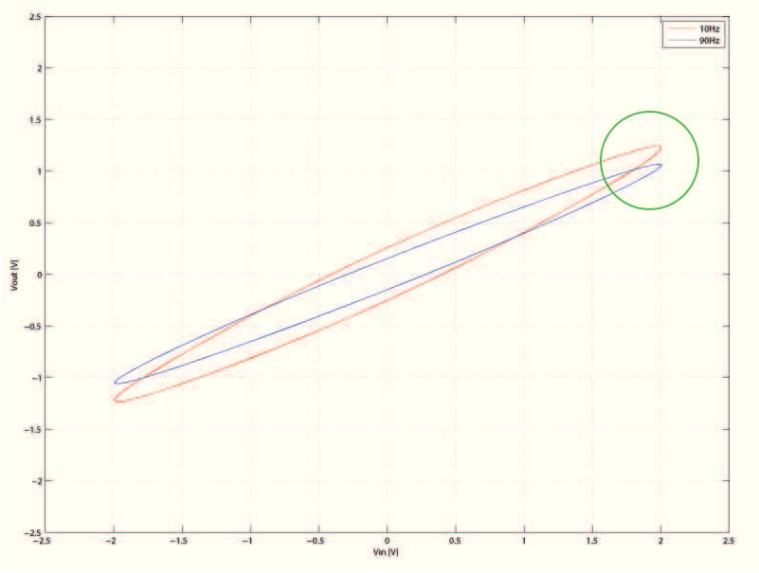

Fig. 3.25. $FOE_{0.002}$ Lissajous curves on measured V_{in} and V_{out} voltages at frequency $10Hz$ (purple) and $90Hz$ (blue).

and phase) in both three cases. In Tab. 3.3 the obtained value are reported.

	α_{gain}	α_{phase}
FOE_{0005}	0.0123	0.0057
FOE_{001}	0.0084	0.0039
FOE_{002}	0.0046	0.0013

Table 3.3. α values referred to different PVP concentrations.

In Fig. 3.26 the evaluated α_{gain} and α_{phase} in relation with the PVP concentration variation are shown and analyzing the plots, the following two linear approximations of the fractional exponent related to the PVP concentration was obtained:

$$\alpha_{gain} = -5.13 PVP_{mol} + 0.01486 \tag{3.10a}$$

$$\alpha_{phase} = -2.93 PVP_{mol} + 0.00716 \tag{3.10b}$$

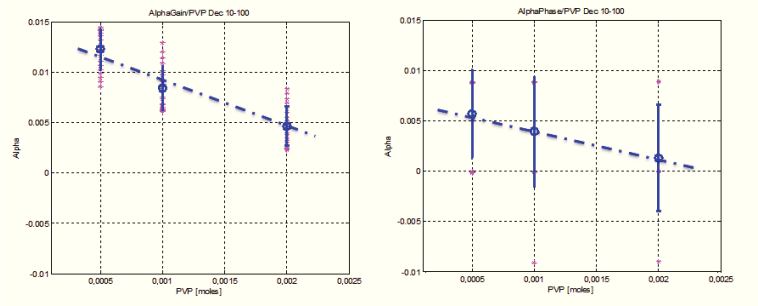

Fig. 3.26. Variation of α_{gain} (on the left) and α_{phase} (on the right) referred to PVP concentration.

With the (3.10a) and (3.10b) it was obtained a linear relationship between the concentration of dispersing agent (PVP) used in the manufactory process and the fractional order of the devices produced.

4

Concluding remarks

This Ph.D. Thesis was focused on Fractional Order Control and Fractional Order Elements. The main goal was to highlight the new role of Non-Integer Order Systems in the area of control engineering and circuits. In the first chapter an introduction on fractional order systems and an overview on the main principles of fractional calculus has been reported. In the next parts the thesis describes different application of such systems. The second chapter was dedicated to the introduction of an effective auto-tuning procedure for $PI^{\lambda}D^{\mu}$ controllers and their analog and digital applications. The third chapter proposed an innovative model of Ionic Polymer Metal Composites (IPMCs) devices and their control. These models are able to better describe the behavior of this polymer that are particularly attractive for possible applications in different fields, such as robotics, aerospace, biomedicine, etc. In the same chapter two analysis on manufactory parameters choice for IPMCs fabrication as Fractional Order Elements (FOEs) has been proposed. In particular the absorption time and dispersing agent concentration parameters have been considered. These results represent a

first steps toward a simplified model of IPMC as a compact electronic FOE by defining the relationship between fabrication parameters, as the absorption time and the dispersing agent concentration with the fractional exponent and the bandwidth. These devices could represent the starting building vlock for the implementation of analog fractional order controllers.

Acknowledgements

Una vita senza ricerca non é degna di essere vissuta.

(Socrate, 399/388 a.C.)

This Thesis concludes four years of work in which any opportunities were derived from this experiences, first of all the birth of some sincere friendships and also the possibility to compare my knowledge and experiences with other researches and colleagues. One of the biggest satisfaction of this last four years in University of Catania derived from this Ph.D. experience is the birth of an Academic Spin-off of the University of Catania called *HIBAS S.r.L.* that operate in the home and building automation systems that represents also a big dream became reality.

For all of this I have to thanks Prof. Riccardo Caponetto, that from Tutor for this Ph.D. course has become also a colleague in HIBAS S.R.L. and gave me the possibility to create it, Prof. Salvatore Graziani to have been a helpful and supporting figure in many troubles of my research activity and last but not least Prof. Luigi Fortuna, the Coorinator of

the Ph.D. Course, for the given support and the constant guide in the years from my first level Bachelor's degree to today.
The biggest thanks, risking to becoming obvious and oversentimental, go to my Family that supplied me in all of my choices and gave me the possibility to become the man who now I am and to Valentina, who most of all represents a big support, a guide and a great love.
The last thank goes to a person that in every troubles and difficulties believed in me and gave me the strength to pass through: Me!

References

1. R. Caponetto, G. Dongola, L. Fortuna, I. Petráš, *Fractional Order Systems: Modeling and Control Applications*, World Scientific Series on Nonlinear Science Series A: Volume 72, February 2010.
2. R. L. Magin, M. Ovadia, *Modeling the cardiac tissue electrode interface using fractional calculus*, Journal of Vibration and Control, vol. 14, no. 9-10, pp. 1431-1442, 2008.
3. L. Sommacal, P. Melchior, A. Oustaloup, J. M. Cabelguen, A. J. Ijspeert, *Fractional multi-models of the frog gastrocnemius muscle*, Journal of Vibration and Control, vol. 14, no. 9-10, pp. 1415-1430, 2008.
4. A.A. Kilbas, H.M. Srivastava, J.J. Trujillo, *Theory and Applications of Fractional Differential Equations*, North-Holland Mathematics Studies, vol. 204, Elsevier, 2006.
5. N. Heymans, *Dynamic measurements in long-memory materials: fractional calculus evaluation of approach to steady state*, Journal of Vibration and Control, vol. 14, no. 9-10, pp. 1587-1596, 2008.
6. J. De Espindola, C. Bavastri, E. De Oliveira Lopes, *Design of optimum systems of viscoelastic vibration absorbers for a given material based on the fractional calculus model*, Journal of Vibration and Control, vol. 14, no. 9-10, pp. 1607-1630, 2008.
7. M. F. M. Lima, J. A. T. Machado, M. Crisostomo, *Experimental signal analysis of robot impacts in a fractional calculus perspective*, Journal of Advanced Computational Intelligence and Intelligent Informatics, vol. 11, no. 9, pp. 1079-1085, 2007.
8. J. Rosario, D. Dumur, J. T. Machado, *Analysis of fractional-order robot axis dynamics*, Proceedings of the 2nd IFAC Workshop on Fractional Differentiation and Its

Applications, vol. 2, July 2006.

9. L. Debnath, *Recent applications of fractional calculus to science and engineering*, International Journal of Mathematics and Mathematical Sciences, vol. 2003, no. 54, pp. 3413-3442, 2003.
10. G. W. Bohannan, *Analog fractional order controller in temperature and motor control applications*, Journal of Vibration and Control, vol. 14, no. 9-10, pp. 1487-1498, 2008.
11. J. Cervera, A. Banos, *Automatic loop shaping in QFT using CRONE structures*, Journal of Vibration and Control, vol. 14, no. 9-10, pp. 1513-1529, 2008.
12. I. Podlubny, *Fractional Differential Equations: An Introduction to Fractional Derivatives, Fractional Differential Equations, to Methods of Their Solution and Some of Their Applications*, Mathematics in Science and Engineering, vol. 198, 1999.
13. R. Panda, M. Dash, *Fractional generalized splines and signal processing*, Signal Processing, vol. 86, no. 9, pp. 2340-2350, 2006.
14. Z.-Z. Yang, J.-L. Zhou, *An improved design for the IIR-type digital fractional order differential filter*, Proceedings of the International Seminar on Future BioMedical Information Engineering (FBIE 08), pp. 473-476, December 2008.
15. V.V. Vasil'ev, L.A. Simak, *Fractional Calculus and Approximation Methods in Modelling of Dynamic Systems*, NAS (Nat. Acad. Sci.) of Ukraine, Kiev, 2008.
16. V. Lakshmikantham, S. Leela, J. Vasundhara Devi, *Theory of Fractional Dynamic Systems*, Cambridge Scientific Publishers, Cambridge, 2009.
17. I. Petráš, *A note on the fractional-order cellular neural networks*, Proceedings of the International Joint Conference on Neural Networks, pp. 1021-1024, July 2006.
18. L. Dorcak, I. Petras, I. Kostial, J. Terpak, *Fractional-order state space models*, Proceedings of the International Carpathian Control Conference, pp. 193-198, 2002.
19. D. Cafagna, *Past and present fractional calculus: a mathematical tool from the past for present engineers*, IEEE Industrial Electronics Magazine, vol. 1, no. 2, pp. 35-40, 2007.
20. K.B. Oldham, J. Spanier, *Fractional Calculus*, Academic Press, N.Y., 1974.
21. B. Ross, *Fractional Calculus and its Applications*, SpringerVerlag, Berlin, 1975.
22. I. Podlubny, *Fractional order systems and $PI^{\lambda}D^{\mu}$ controler*, IEEE Transaction on Automatic Control, 44(2), pp. 208-214, 1999.

23. C. Ma, Y. Hori, *Fractional order control and its application of $PI^{\alpha}D$ controller for robust twoinertia speed control*, Proceedings of the 4^{th} International Power Electronics and Motion Control Conference (IPEMC 04), vol. 3, pp. 1477-1482, August 2004
24. K. B. Oldham, J. Spanier, *The Fractional Calculus: Theory and Applications of Differentiation and Integration to Arbitrary Order*, Dover Books on Mathematics, 2006.
25. J. A. T. Machado, *A probabilistic interpretation of the fractional-order differentiation*, Fractional Calculus and applied Analysis, vol. 6, no. 1, pp. 73-80, 2003.
26. D. Baleanu, S. I. Muslih, *Nonconservative systems within fractional generalized derivatives*, Journal of Vibration and Control, vol. 14, no. 9-10, pp. 1301-1311, 2008.
27. T. Poinot, J.-C. Trigeassou, *A method for modelling and simulation of fractional systems*, Signal Processing, vol. 83, no. 11, pp. 2319-2333, 2003.
28. R. Caponetto, D. Porto, *Analog implementation of non integer order integrator via field programmable analog array*, Proceedings of the 2^{nd} IFAC Workshop on Fractional Differentiation and Its Applications, vol. 2, July 2006.
29. T. C. Haba, G. Ablart, T. Camps, F. Olivie, *Influence of the electrical parameters on the input impedance of a fractal structure realised on silicon*, Chaos, Solitons and Fractals, vol. 24, no. 2, pp. 479-490, 2005.
30. W. Kaplan, *Advanced Calculus*, 4^{th} ed. Reading, MA: Addison Wesley, 1992.
31. A. Oustaloup, *Systemes asservis lineares d'ordre fractionnaire*, Masson, Paris, 1983.
32. P. Arena, L. Bertucco, L. Fortuna, G. Nunnari, D. Porto, *CNN with Non-integer order cells*, 5^{th} IEEE International Workshop on Cellular Neural Networks (CNNA 98), London, Great Britain, pp. 372-378, April 1998.
33. R. Caponetto, G. Dongola, F.L. Pappalardo, V. Tomasello, *Autotuning Method for $PI^{\lambda}D^{\mu}$ Controllers Design*, International Journal of Innovative Computing, Information and Control, vol. 9, num. 10, pp. 4043-4055, 2013.
34. R. Caponetto, G. Dongola, F.L. Pappalardo, V. Tomasello, *Auto-Tuning and Fractional Order Controller Implementation on Hardware in the Loop System*, J. Optim. Theory Appl., vol. 156, pp. 141-152, 2013.
35. A. Oustaloup, M. Bansard, *First generation CRONE control*, Proc. International Conference on Systems, Man and Cybernetics, 1993.
36. A. Oustaloup, P. Lanusse, B. Mathieu, *Second generation CRONE control*, Proc. International Conference on Systems, Man and Cybernetics, 1993.

37. A. Oustaloup, P. Lanusse, B. Mathieu, *Third generation CRONE control*, Proc. International Conference on Systems, Man and Cybernetics, 1993.
38. B.M. Vinagre, C.A. Monje, V. Feliu, Y. Chen, *On Auto-Tuning of Fractional Order $PI^{\lambda}D^{\mu}$ Controllers*, Proc. IFAC Workshop on Fractional Differentiation and its Application (FDA 06), Porto, Portugal, 2006.
39. R. Caponetto, D. Porto, *Analog implementation of non integer order integrator via field Programmable Analogic array*, IFAC Workshop on Fractional Differentiation and its Application, Porto, 19-21 July 2006.
40. R. Caponetto, G. Dongola, *Field Programmable Analog Array Implementation of Non Integer Order $PI^{\lambda}D^{\mu}$ Controller*, Journal of Computational and Nonlinear Dynamics, vol. 3, April 2008.
41. A. Datta , M.T. Ho , S.P. Bhattacharyya, *Structure and Synthesis of PID Controller*, London, United Kingdom, Springer-Verlag, 2000.
42. L.S. Pontryagin, *On the zeros of some elementary transcendental function*, Amer. Math. Society Translation, vol. 2, pp. 95-110, 1955.
43. J.S. Karmarkar, D.D. Siljak, *Stability analysis of systems with time delay*, Proc. IEE, vol. 117, no. 7, pp. 1421-1424, July 1970.
44. G.J. Silva, A. Datta, S.P. Bhattacharyya, *New Results on the Synthesis of PID Controllers*, IEEE Trans. Automat. Contr., vol. 47, n. 2, February 2002.
45. R. Caponetto, L. Fortuna, D. Porto, *Parameter tuning of a non-integer order PID controller*, The 15^{th} International Symposium on Mathematical Theory of Networks and Systems, Notre Dame, Indiana, 2002.
46. R. Caponetto, L. Fortuna, D. Porto, *A new tuning strategy for non integer order PID controller*, The 1^{st} IFAC Workshop on Fractional Differentiation and Its Application, Bordeaux, France, 2004.
47. Y.Q. Chen, B.M. Vinagre, C. Monje, *A proposition for the implementation of non-integer PI controllers*, In Thematic actionsystems with non-integer derivations, Bordeaux, France, 2003.
48. C. Monje, A. Calderón, B.M. Vinagre, *PI vs fractional DI control: First results*, In CONTROL 2002: 5^{th} Portuguese conference on automatic control, Aveiro, Portugal, pp.359-364, 2002.

49. A. Monje, B.M. Vinagre, V. Feliu, Y. Chen, *Tuning and auto-tuning of fractional order controllers for industry applications*, Control Engineering Practice, vol.16, pp.798-812, 2008.
50. M. Caputo, *Linear model of dissipation whose Q is almost frequency independent-II*, Geophys. J. R. Astr. Soc., vol. 13, pp. 529-539, 1967.
51. M. Caputo, *Elasticita e Dissipacione*, Bologna: Zanichelli, 1969.
52. G.E. Santamaria, I. Tejado, B.M. Vinagre, A. Monje, *Fully Automated and Tuning and implementation of Fractional PID Controllers*, California, USA, vol.DETC 2009-87399, 2009.
53. K.B. Oldham, J. Spanier, *The Fractional Calculus: Theory and Applications of Differentiation and Integration to Arbitrary Order*, Dover Books on Mathematics, 2006.
54. M.Shahinpoor, K.J. Kim, *Ionic polymer metal composites: I. Fundamentals*, Smart Mater. Struct., vol. 10, pp. 819-833, 2001.
55. B. Andó, S. Graziani, *Plasticland: where a new world comes true.*, IEEE Instrumentation and Measurement Magazine, 12-6, 30-35, 2009.
56. P. Brunetto,L. Fortuna, P. Giannone, S. Graziani, S. Strazzeri, *Static and Dynamic Characterization of the Temperature and Humidity Influence on IPMC Actuators*, IEEE Trans. Inst. and Meas., no. 59, vol. 4, pp. 893-908, 2010.
57. K. Mallavarapu, D.J. Leo, *Feedback Control of the vending response of Ionic Polymer Actuators*, J. of Int. Mat. Sys. and Struc., vol. 12, pp. 143-155, 2001.
58. B.C. Lavu, M.P. Schoen, A. Mahjan, *Adaptive intelligent control of ionic polymer-metal composites*, Smart Materials and Structures, vol. 14, pp. 466-474, 2005.
59. J. Brufau-Penella, K. Tsiakmakis, T. Laopoulos, M. Puig-Vidal, *Model reference adaptive control for an ionic polmer metal composite in underwater applications*, Smart Materials and Structures, vol. 17, n. 4, pp. 9, 2008.
60. C. Bonomo, L. Fortuna, P. Giannone, S. Graziani, S. Strazzeri, *A nonlinear model for ionic polymer metal composites as actuators*, Smart Materials and Structures, vol. 16, pp. 1-12, 2007.
61. X. Bao, Y. Bar-Cohen, S. Lih, *Prociding of SPIES Smart Structures and Materials Symposium*, EAPAD Conference, San Diego, California, 4695-27, 2002.
62. R. Caponetto, G. Dongola, L. Fortuna, S. Graziani, S. Strazzeri, *A Fractional Model for IPMC Actuators*, IEEE International Instrumentation adn Measurement Technology Conference, Canada, 2008.

63. DuPont website, *The History of Teflon*, on web at *http : //www. − dupont.com/teflon/newsroom/history.html*.
64. K. Oguro, on web at *http : //ndeaa.jpl.nasa.gov/nasa − nde/lommas/eap/IPMC$_P$repProcedure.htm*.
65. S. Nemat-Nasser, Y.X. Wu, *Comparative experimental study of ionic polymermetal composites with different vackvone ionomers and in various cation forms*, J. Appl. Phys., vol.93-9, pp. 5255-5267, 2003.
66. R. Caponetto, *Non-linear non-integer order circuits and systems*, World Scientific Book, World Scientific Series On Nonlinear Science Series A, 2000.
67. S. Tadokoro, S. Yamagami, *Modeling of nafion-pt composite actuators (icpf) by ionic motion*, in Proc. of SPIES, 2, 2000.
68. S. Nemat-Nasser, *Micromechanics of actuation of ionic polymer-metal composites*, J. Appl. Phys., vol. 92, pp. 2899-2915, 2002.
69. Y. Xiao, K. Bhattacharya, *Modeling electromechanical properties of ionic polymers*, in Proc. of SPIES, 4329, pp. 292-300, 2001.
70. R. Kanno, K. Oguro, *Characteristics and modeling of icpf actuators*, in Proc. of Japan-USA Symp. on Flexivle Automation, vol. 2, 691-8, 1994.
71. S. Nemat-Nasser, J.Y. Li, *Electromechanical response of ionic polymer-metal composites*, J. Appl.Phys., vol. 87, pp. 3221-3331, 2000.
72. K. Newbury, *Ph.D. dissetation*, Virginia Polytechnic Institute and State University, 2002.
73. C. Bonomo, S. Strazzeri, *A model for ionic polymer metal composite as sensor*, IOP Smart Materials and Structures, vol. 15, pp. 749-758, 2006.
74. K. Newbury, D. Leo, *Linear electromechanical model of ionic polymer transucers - part I: Model development*, Journal of Intelligent Material Systems and Structures, vol. 14, pp. 333-342, 2003.
75. L. Chang, H. Chen, Z. Zhu, *A structure model for Ionic polymer-metal composite(IPMC)*, in Proc. of SPIE in Electroactive Polymer Actuators and Devices (EAPAD 12), vol. 8340, April 2012.
76. R. Caponetto, S. Graziani, F.L. Pappalardo, E. Umana, M.G. Xibilia, P. Di Giambernardino, *A Scalable Fractional Order Model for IPMC Actuators*, in Proc. MathMod12, Vienna, Austria, 2012.

77. R. Caponetto, S. Graziani, F.L. Pappalardo, M.G. Xibilia, *Parametric Control of IPMC Actuator Modeled as Fractional Order System*, Advances in Science and Technolofy, vol. 79, pp. 63-68, 2013.
78. R. Caponetto, G. Dongola, F.L. Pappalardo, *Modeling and Control of IPMC actuator*, in Proc. of the Fifth IFAC Workshop on Fractional Differentiation and its Applications (FDA12), Nanjiing, China, May 2012.
79. R. Caponetto, S. Graziani, F.L. Pappalardo, M.G. Xibillia, *A comparison between robust and parameterized controllers for fractional order modeled Ionic Polymeric Metal Composite actuator*, 6^{th} Workshop on Fractional Differentiation and Its Applications Part of 2013 IFAC Joint Conference SSSC Grenoble, Grenoble, France, February 2013.
80. R. Caponetto, G. Dongola, L. Fortuna, I. Petras, *Fractional Order Systems: Modelling and Control Applications*, Nonlinear Science, Series A - vol. 72, World Scientific, Singapore, 2010.
81. D.W. Marquardt, *An Algorithm for Least-Squares Estimation of Nonlinear Parameters*, Journal of the Society for Industrial and Applied Mathematics, vol. 11-2, pp. 431-441, 1963.
82. R. Caponetto, S. Graziani, F.L. Pappalardo, F. Sapuppo, *Experimental Characterization of Ionic Polymer Metal Composite as a Novel Fractional Order Element*, Special Issue on Advanced Topics in Fractional Dynamics, Advances in Mathematical Physics, October 2013.
83. R. Caponetto, S. Graziani, F.L. Pappalardo, F. Sapuppo, *A Ionic Polymer Metal Composite Fractional Order Element*, in Proc. of International Conference on Fractional Differentiation and Its Applications (ICFDA 14), Catania, Italy, June 2014.